

Galactic-Centre Gamma Rays in CMSSM Dark Matter Scenarios

John Ellis^{1,2}, Keith A. Olive³ and Vassilis C. Spanos⁴

¹*TH Division, Physics Department, CERN, CH-1211 Geneva 23, Switzerland*

²*Theoretical Particle Physics and Cosmology Group, Physics Department,
King's College London, London WC2R 2LS, UK*

³*William I. Fine Theoretical Physics Institute & Department of Physics,
University of Minnesota, Minneapolis, MN 55455, USA*

⁴*Institute of Nuclear Physics, NCSR "Demokritos", GR-15310 Athens, Greece*

Abstract

We study the production of γ rays via LSP annihilations in the core of the Galaxy as a possible experimental signature of the constrained minimal supersymmetric extension of the Standard Model (CMSSM), in which supersymmetry-breaking parameters are assumed to be universal at the GUT scale, assuming also that the LSP is the lightest neutralino χ . The part of the CMSSM parameter space that is compatible with the measured astrophysical density of cold dark matter is known to include a $\tilde{\tau}_1 - \chi$ coannihilation strip, a focus-point strip where χ has an enhanced Higgsino component, and a funnel at large $\tan\beta$ where the annihilation rate is enhanced by the poles of nearby heavy MSSM Higgs bosons, A/H . We calculate the total annihilation rates, the fractions of annihilations into different Standard Model final states and the resulting fluxes of γ rays for CMSSM scenarios along these strips. We observe that typical annihilation rates are much smaller in the coannihilation strip for $\tan\beta = 10$ than along the focus-point strip or for $\tan\beta = 55$, and that the annihilation branching ratios differ greatly between the different dark matter strips. Whereas the current Fermi-LAT data are not sensitive to any of the CMSSM scenarios studied, and the calculated γ -ray fluxes are probably unobservably low along the coannihilation strip for $\tan\beta = 10$, we find that substantial portions of the focus-point strips and rapid-annihilation funnel regions could be pressured by several more years of Fermi-LAT data, if understanding of the astrophysical background and/or systematic uncertainties can be improved in parallel.

1 Introduction

Relatively soon after the realization that the lightest supersymmetric particle (LSP), in particular the lightest neutralino χ , could naturally provide the astrophysical dark matter in models in which R -parity is conserved [1], it was suggested that LSP dark matter annihilations might be detectable via features in the γ -ray spectrum [2]. This is now a hot theoretical [3–11] and experimental topic, with several experiments [12–19] studying the cosmic-ray γ spectra from a variety of astrophysical sources such as the galactic centre and bulge as well as dwarf galaxies. There have been claims of deviations from calculations of conventional γ -ray backgrounds, and corresponding claims of evidence for new physics invoking tailor-made supersymmetric scenarios [20]. In parallel, particularly in the context of searches with accelerator experiments, there have been many studies of simplified supersymmetric scenarios. Foremost among such scenarios is the constrained minimal supersymmetric extension of the Standard Model (CMSSM), in which the soft supersymmetry-breaking parameters m_0 , $m_{1/2}$ and A_0 are assumed to be universal at the supersymmetric GUT scale [21–26].

Accelerator experiments and astrophysical searches have complementary roles to play in elucidating the nature of any dark matter particles. Accelerator experiments cannot determine whether any candidate dark matter particle is in fact stable, rather than merely living long enough to escape from the apparatus, while astroparticle experiments are limited in their capabilities to disentangle the dynamics of dark matter models and thereby, for example, verify that they yield the appropriate cosmological dark matter density. Connecting the accelerator and astroparticle experiments requires interpreting them within a common model framework, and in this paper we choose to compare their sensitivities within the framework of the CMSSM, assuming that R -parity is conserved and that the LSP is the lightest neutralino χ .

The parameters of the CMSSM are the universal scalar mass m_0 , gaugino mass $m_{1/2}$ and trilinear supersymmetry-breaking parameter A_0 , the ratio of Higgs vevs $\tan\beta$ and the sign of the Higgs mixing parameter μ . Here we focus on $\mu > 0$, motivated by $g_\mu - 2$ [27, 28] and (to a lesser extent) by $b \rightarrow s\gamma$ [29]. We study the cases $\tan\beta = 10, 55$, which bracket the phenomenologically-plausible range. Currently, there is little experimental sensitivity to A_0 , and we limit our discussion here to the case $A_0 = 0$.

As is well known, the regions of the CMSSM parameter space in which the dark matter density falls within the narrow range permitted by WMAP and other cosmological observations [30] may be represented as relatively narrow strips in $(m_{1/2}, m_0)$ planes for fixed values of $\tan\beta$ [25, 31], which are illustrated in Fig. 1. As seen in the left panel, if $\tan\beta = 10$ there

is one WMAP strip with $m_0 \ll m_{1/2}$ where the relic density is reduced into the allowed range by coannihilations of the relic neutralinos χ with sleptons $\tilde{\ell}$ [32], and another strip at relatively large m_0 in the so-called ‘focus-point’ region [33] where the relic density is brought into the allowed range by enhanced annihilation due to a relatively large Higgsino component in the composition of the lightest neutralino χ . If $\tan\beta = 55$, as seen in the right panel of Fig. 1, the coannihilation strip segues into a funnel region [21, 23] where the relic density is brought into the allowed range by rapid annihilations through direct-channel heavy Higgs resonances H/A . Also visible in Fig. 1 are the constraints imposed by $b \rightarrow s\gamma$, the LEP lower limits on chargino and Higgs masses [34], and the region favoured by $g_\mu - 2$ if the apparent experimental discrepancy with the Standard Model calculation is ascribed to supersymmetry. Fig. 1 also shows the constraints implied by the absence of any supersymmetric signal in the 2010 LHC data [35].

In this paper we study the likely sensitivity of searches for γ rays from the galactic centre to LSP annihilations in the CMSSM, taking as examples the $(m_{1/2}, m_0)$ planes shown in Fig. 1 and focusing on the dark blue WMAP strips, in particular. The first step is to understand relevant features of CMSSM dark matter annihilation processes, which we study in Section 2. As we discuss there, the $\chi - \chi$ annihilation cross section is much smaller in the coannihilation region of the CMSSM for $\tan\beta = 10$ than it is in the focus-point region, or for $\tan\beta = 55$. This is easily understood, because in the $\tan\beta = 10$ coannihilation strip the relic density is brought down into the WMAP range by the sum over all $\chi - \tilde{\ell}$ coannihilation processes, relative to which $\chi - \chi$ annihilation is numerically small. Moreover, only S-wave annihilation is important in the Universe today, whereas P-wave annihilation also played a role in the early Universe, particularly for the parameter space associated with the co-annihilation strip. The smallness of the S-wave $\chi - \chi$ annihilation cross section in the $\tan\beta = 10$ coannihilation strip implies that all astroparticle searches for dark matter annihilation products, whether they be photons, neutrinos, positrons, antiprotons or antideuterons, will be relatively insensitive in this region of the CMSSM parameter space.

A second issue we study in Section 2 is that of the branching fractions for annihilations into different final Standard Model states. Indicative explorations of annihilation signatures may assume particular final states as illustrations, but in the CMSSM these branching fractions are fixed at each point in parameter space. We find that the dominant annihilation channels are $\tau^+\tau^-$ in the coannihilation region and W^+W^- in the focus-point region for $\tan\beta = 10$, and $\bar{b}b$ in both regions for $\tan\beta = 55$. The $\gamma\gamma$ final state, which would be particularly promising for detection via a γ line with $E_\gamma = m_\chi$, unfortunately has a very small branching fraction in all cases. The next step is to model the hadronic, leptonic and

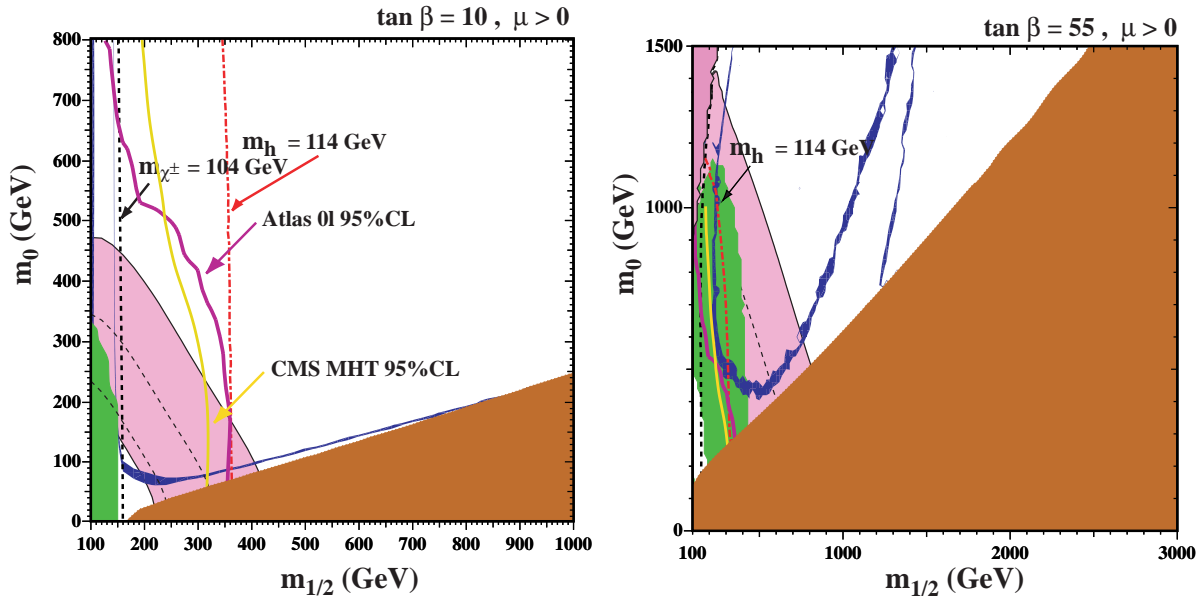


Figure 1: The $(m_{1/2}, m_0)$ planes in the CMSSM for $\tan \beta = 10$ (left) and $\tan \beta = 55$ (right), assuming $\mu > 0$ and $A_0 = 0$, showing the 95% CL limits imposed by ATLAS and CMS data (purple and yellow lines, respectively). The regions where the relic LSP density falls within the range allowed by WMAP and other cosmological observations appear as strips shaded dark blue. The constraints due to the absences of charginos and the Higgs boson at LEP are also shown, as black dashed and red dot-dashed lines, respectively. Regions excluded by the requirements of electroweak (EW) symmetry breaking and a neutral LSP are shaded dark pink and brown, respectively. The green region is excluded by $b \rightarrow s\gamma$, and the pink region is favoured by the supersymmetric interpretation of the discrepancy between the Standard Model calculation and the experimental measurement of $g_\mu - 2$ within ± 1 and ± 2 standard deviations (dashed and solid lines, respectively).

γ components of the final states, for which we use PYTHIA, as introduced at the end of Section 2.

In Section 3, we turn to the treatment of the astrophysical background and astrophysical aspects of indirect detection. In particular, we discuss possible dark matter profiles towards the center of the galaxy, including Navarro-Frenk-White (NFW) [36] and Einasto models [37, 38], as well as a simple isothermal model [39]. We also compare our predicted signal with a model background and the current data and possible sensitivity of the Fermi-LAT detector [13] in Section 3, illustrating our discussion with some specific benchmark CMSSM scenarios. Then, in Section 4, we present estimates of the perspectives Fermi-LAT may have for distinguishing a possible annihilation γ -ray signature from the background along the WMAP strips shown in Fig. 1. As might be expected on the basis of the magni-

tudes of the annihilation cross sections in the different regions of CMSSM parameter space, for $\tan\beta = 10$ there are better prospects for disentangling a signal from the background in the focus-point region, whereas for $\tan\beta = 55$ there are prospects in both the funnel and focus-point regions. However, putting pressure on the CMSSM scenarios studied here with future years of Fermi-LAT data would require considerable improvements in the modelling of the background and/or reduction in the systematic errors. Section 5 summarizes our conclusions about searches for γ rays from the galactic centre, and makes some remarks about other search strategies for CMSSM dark matter annihilations.

2 CMSSM Dark Matter Annihilation Processes

The relic density of neutralinos is determined by annihilations when they are slightly non-relativistic. Typically, annihilation freeze-out occurs when $x \equiv T/m_\chi \sim v_{\text{rel}}^2/6 \sim 1/23$, where v_{rel} is the relative velocity of annihilating particles and T is the temperature of the Universe. For small $x < 1$, the annihilation cross section can be expanded in a series as $\langle\sigma v_{\text{rel}}\rangle = a + bx + \dots$ [1, 40]. Because neutralinos are Majorana particles, we generally have $a \propto m_f^2/m_{\text{susy}}^4$, where m_f is the mass of a final-state fermion, and $b \propto m_\chi^2/m_{\text{susy}}^4$. Hence, often $a \ll b$ and the relic density is largely determined by b , with higher-order coefficients in the expansion relatively unimportant. Any signal of dark matter annihilations will also be scaled by the annihilation cross section. However, since dark matter particles annihilating in the galactic halo today are very non-relativistic with $v_{\text{rel}} \ll 1$, the annihilations are essentially pure S-wave, and $\langle\sigma v_{\text{rel}}\rangle \approx a$. This is a valid argument even close to the inner region of the galactic halo, where the N-body simulations indicate that the DM halo particles are quite non-relativistic, with $v_{\text{rel}} \sim \mathcal{O}(10^{-4} - 10^{-3})$ [36].

We note in passing that in our calculation the Sommerfeld enhancement effect [41] is not important. One condition for having such a sizeable enhancement is a high degree of mass degeneracy between the LSP and another sparticle, such as the chargino or stau. However, along the focus-point WMAP strip it is not possible to achieve the required amount of degeneracy between the LSP and lightest chargino and, on the other hand, along the stau coannihilation strip the effect of the Sommerfeld enhancement is known not to be important [42].

With this in mind, we display in Fig. 2 the S-wave $\chi - \chi$ annihilation cross section along the WMAP-compatible strips shown in Fig. 1, as a function of $m_{1/2}$ in each case. The coannihilation/funnel strips are represented by solid lines, black for $\tan\beta = 10$ and red for $\tan\beta = 55$, and the focus-point strips are represented by a blue dotted line for $\tan\beta = 10$

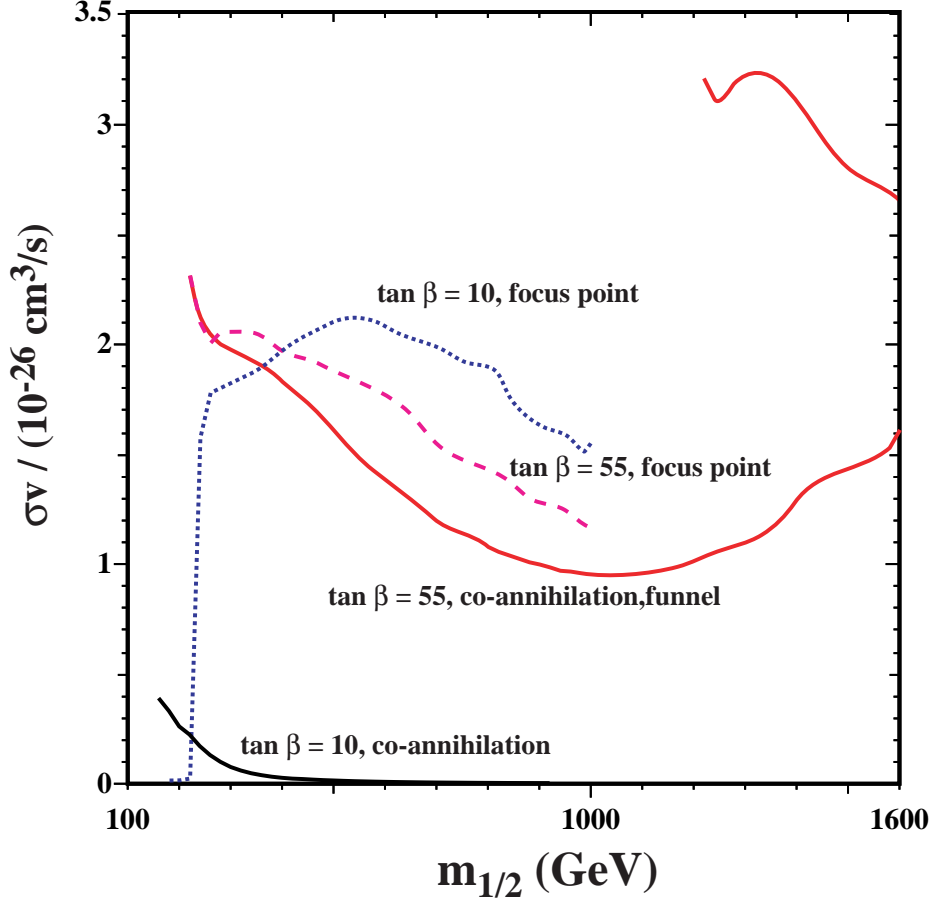


Figure 2: The $\chi - \chi$ annihilation cross section along the WMAP strips in the coannihilation, focus-point and funnel regions for $\tan \beta = 10, 55$, $A_0 = 0$ and $\mu > 0$, as functions of $m_{1/2}$. We see that the annihilation cross section along the $\tan \beta = 10$ coannihilation strip is much smaller than along the other strips, and decreases rapidly as $m_{1/2}$ increases.

and a mauve dashed line for $\tan \beta = 55$. In each case, we have fixed $A_0 = 0$ and for each value of $m_{1/2}$ we have adjusted the value of m_0 to obtain the WMAP value of the relic density, $\Omega_\chi h^2 = 0.1109 \pm 0.0056$ [30].

We notice immediately that the total $\chi - \chi$ annihilation cross section is much smaller along the coannihilation strip for $\tan \beta = 10$ than in the other cases, falling rapidly as $m_{1/2}$ increases. This reflects the importance of $\chi - \tilde{\ell}$ coannihilations in reducing the cosmological relic density into the WMAP-compatible range, a role that becomes increasingly important at larger $m_{1/2}$ where the χ and $\tilde{\tau}_1$ are increasingly degenerate. We recall that, as seen in Fig. 1, the LHC upper limits on sparticle production enforce $m_{1/2} > 350$ GeV along this strip, where $\sigma v < 10^{-27}$ cm³/s, whereas $g_\mu = 2$ favours the portions of the coannihilation

strips with $m_{1/2} < 400$ GeV for $\tan\beta = 10$ and $m_{1/2} < 800$ GeV for $\tan\beta = 55$.

On the other hand, the total S-wave annihilation cross section is much larger along the other WMAP strips shown in Fig. 2, with typically $\sigma v \sim (1 - 2) \times 10^{-26}$ cm³/s¹. This difference immediately suggests that detecting dark matter annihilations will be easier along the funnel for $\tan\beta = 55$ as well as the focus-point strip for $\tan\beta = 10$, or for $\tan\beta = 55$. We note, however, that these regions are disfavoured by fits to $g_\mu - 2$ and other low-energy precision observables [43].

In the case of the coannihilation/funnel strip for $\tan\beta = 55$, we note the appearance of a second red line for $m_{1/2} > 1200$ GeV. This reflects the appearance in Fig. 2 of a second branch of the WMAP strip on the other side of the rapid-annihilation H/A funnel seen in the right panel of Fig. 1. The annihilation cross section takes similar values along the focus-point strips for both the $\tan\beta = 10$ and 55 cases (except at small $m_{1/2}$), and the LHC limits have no impact along either of these strips. As seen in Fig. 1, $g_\mu - 2$ favours only the portion of the $\tan\beta = 55$ focus-point strip with $m_{1/2} < 200$ GeV, which is disfavoured by other constraints², and disfavours all the $\tan\beta = 10$ focus-point strip.

The detectability of $\chi - \chi$ annihilation depends also on the branching fractions for annihilations into specific Standard Model final states and the γ spectra they produce. Fig. 3 displays the branching fractions for the most important final states, and we see that they are quite different along the various WMAP strips studied. In the case of the coannihilation strip for $\tan\beta = 10$ (upper left panel), we see that $\tau^+\tau^-$ final states dominate at low $m_{1/2}$, followed by $\bar{b}b$ final states, with W^+W^- and $\bar{t}t$ final states gaining in importance at larger $m_{1/2}$, where the total annihilation cross section is, however, much reduced as seen in Fig. 2.

On the other hand, the roles of the $\bar{b}b$ and $\tau^+\tau^-$ final states are largely reversed along the coannihilation/funnel strip for $\tan\beta = 55$ (upper right panel), including the second branch when $m_{1/2} \sim 1500$ GeV. In the case of the focus-point strip for $\tan\beta = 10$ (lower left panel), we see that W^+W^- final states dominate, except for $\bar{b}b$ final states at small $m_{1/2} \sim 200$ GeV and the appearance of $\bar{t}t$ final states when $m_{1/2} > 400$ GeV. Finally, in the case of the focus-point strip for $\tan\beta = 55$ (lower right panel), we see that $\bar{b}b$ final states dominate over $\tau^+\tau^-$ final states everywhere.

The prompt component of the photon flux, i.e., the photons that are produced directly by neutralino pair annihilation in the halo, consists of two components: the monochromatic and the continuum. The monochromatic component due to the $\gamma\gamma$ branching fraction is very

¹There is an exception at small $m_{1/2}$ on the $\tan\beta = 10$ focus-point strip, where the annihilation $\chi\chi \rightarrow W^+W^-$ is kinematically inaccessible.

²We note that, for $\tan\beta = 55$, the LHC limits have less impact on $m_{1/2}$ than the $b \rightarrow s\gamma$ constraint, which imposes $m_{1/2} > 400$ GeV.

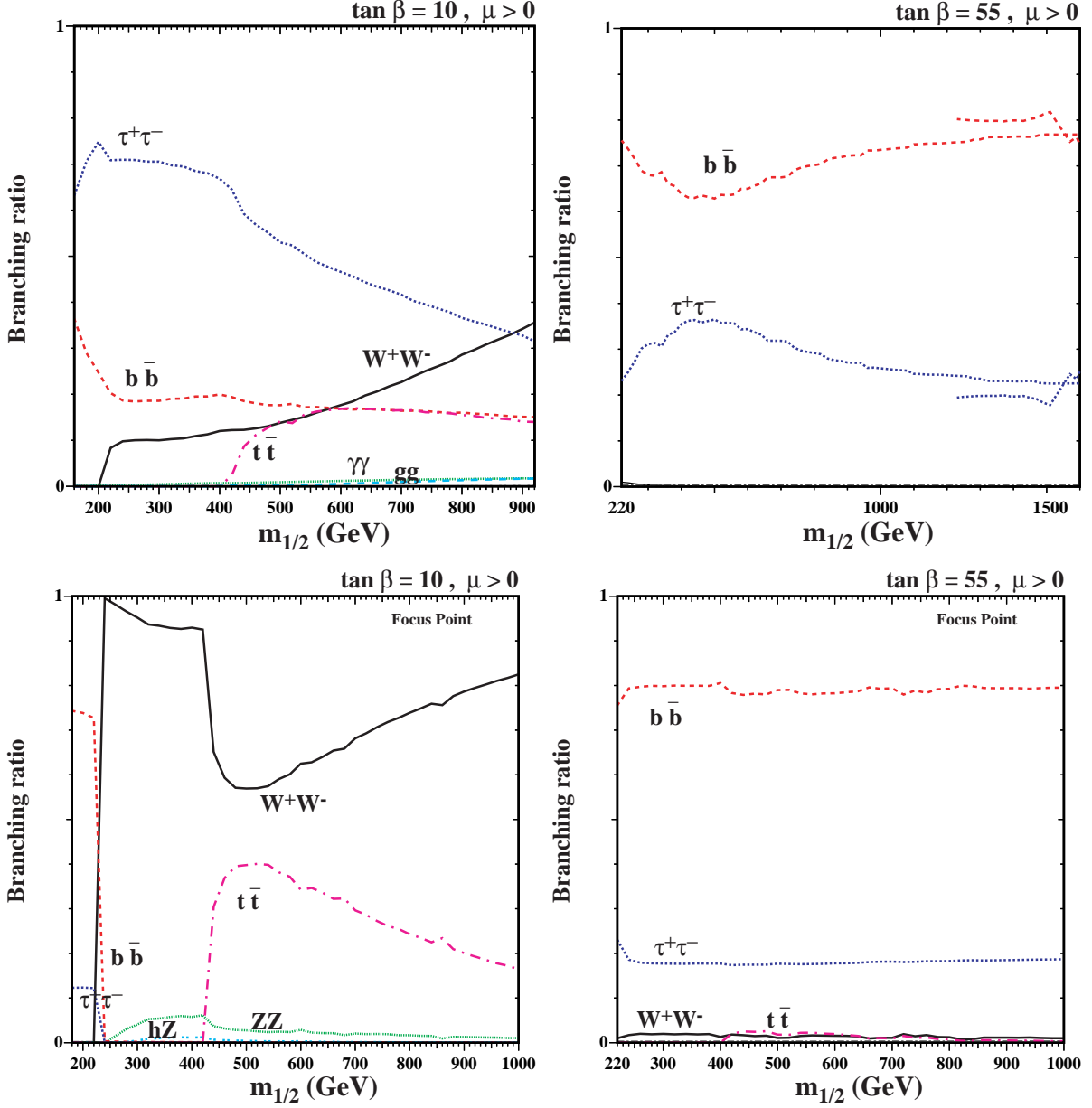


Figure 3: *The branching fractions for $\chi - \chi$ annihilations into pairs of Standard Model particles along the WMAP strips for $\tan \beta = 10$ (left panels) and $\tan \beta = 55$ (right panels), in the coannihilation and funnel regions (upper panels) and in the focus-point region (lower panels).*

small in all cases. For $\tan \beta = 10$, the branching fraction is less than 10^{-3} for $m_\chi \lesssim 400$ GeV. It rises slowly to roughly 0.015 as the endpoint of the coannihilation strip is reached, but here the total annihilation rate is very small, as seen in Fig. 2. In the focus-point region

for $\tan\beta = 10$, the branching ratio is always negligible and remains below 10^{-7} . In the case of the coannihilation/funnel strip for $\tan\beta = 55$ it remains below a few $\times 10^{-5}$, and is even lower along the focus-point strip for $\tan\beta = 55$. Further details, especially for the monochromatic part from the processes $\chi\chi \rightarrow 2\gamma/Z\gamma$, will be given in the next section.

The continuum component is due to photons produced by the multibody neutralino pair annihilation channels, and is usually modelled using event generators such as PYTHIA [44] or HERWIG [45]. Here we use PYTHIA to calculate the continuum component of the differential photon flux dN_{cont}^i/dE_γ . The decay channels we take into account are: $q\bar{q}$ for all quark flavors, and the $\tau^+\tau^-$, W^+W^- , ZZ , gg , Zh and ZH final states³. In particular, we follow [46] and references therein, parametrizing the fits of photon spectra produced by PYTHIA, in order to obtain the differential flux as an analytic function of the parameter $x = E_\gamma/m_\chi$, for each LSP mass m_χ . The functions dN_{cont}^i/dx for each final state are related to the energy spectrum used below $dN_{cont}^i/dE_\gamma = (1/m_\chi)dN_{cont}^i/dx$. Our results for the continuum component agree very well with those of [46, 47]. In the modeled fluxes we have included effects that are related to final state radiation [4]. Recently, it has been shown that final state strong and EW corrections from the radiative emission of gluons, W or Z [48] can enhance otherwise P-wave suppressed channels, like the neutralino pair annihilation to electrons and neutrinos. In principle, corrections to the neutralino annihilation to electrons can affect the photon flux, due to the Inverse Compton Scattering (ICS) effect, but as we will see in the following section, this part of the signal is subdominant for energetic photons.

3 Gamma fluxes and the Fermi-LAT data analysis

In order to estimate the sensitivity of a detector like Fermi-LAT [13] to new sources of photon fluxes arriving from the galactic center (GC), one must calculate both the signal and the background contributions to the photon flux, which we do in the following subsections.

The GC is probably one of the most complicated regions of the Milky Way, from both the observational and the theoretical points of view. Observationally, the emitted electromagnetic spectrum exhibits various interesting features, like the recently-observed giant γ -ray bubbles, the so-called ‘‘Fermi bubbles’’ [49], that can be related to accretion activity. From the theoretical point of view, the supposed existence of a massive black hole in the GC might change drastically the size of the γ -ray flux [7]. Moreover, other phenomena such as turbulent galactic winds, large magnetic fields etc, can affect the theoretical predictions [50]. In

³In the regions of the CMSSM parameter space we study here, the ZH final state, where H is the heavy CP-even Higgs boson, yields a very small contribution.

this work we adopt a conservative approach. In particular, we do not consider the possible effects due to the presence of a massive black hole, or any other source that might enhance the γ -ray flux arising from annihilations of neutralinos in the dark matter halo.

3.1 The supersymmetric signal

In the context of supersymmetric models where the neutralino plays the role of the dark matter particle, there are two main components in the signal:

- Prompt photons produced either directly through one-loop processes such as $2\chi \rightarrow 2\gamma/Z\gamma$ (monochromatic components) or indirectly as final state radiation or through the hadronization, fragmentation and decays of the tree-level neutralino pair annihilation products discussed in the previous section (the continuum component);
- Photons that originate from energetic electrons and positrons produced in neutralino pair annihilation via the Inverse Compton Scattering (ICS) process on background photons.

There is also a synchrotron component produced by the energetic electrons and positrons accelerated in the galactic magnetic field, but it contributes at energies much smaller than the prompt and ICS components [51], below the effective Fermi-LAT threshold. Thus, we may write

$$\left. \frac{d\Phi_\gamma(E_\gamma)}{dE_\gamma} \right|_{signal} = \left. \frac{d\Phi_\gamma(E_\gamma)}{dE_\gamma} \right|_{prompt} + \left. \frac{d\Phi_\gamma(E_\gamma)}{dE_\gamma} \right|_{ICS}, \quad (1)$$

and the total flux $\Phi_\gamma(E_{th})$ as a function of the threshold energy E_{th} is

$$\Phi_\gamma(E_{th}) = \int_{E_{th}}^{m_\chi} dE_\gamma \left. \frac{d\Phi_\gamma(E_\gamma)}{dE_\gamma} \right|_{signal}. \quad (2)$$

In the following, we discuss in detail our calculation of the prompt and the ICS components in the supersymmetric γ signal.

3.1.1 The prompt component

The prompt component may be written as

$$\left. \frac{d\Phi_\gamma(E_\gamma)}{dE_\gamma} \right|_{prompt} = \frac{1}{4\pi} \frac{1}{2 m_\chi^2} \sum_X \frac{dN_\gamma^X}{dE_\gamma} \langle \sigma v \rangle_X \int_{\Delta\Omega} d\Omega \int_{los} \rho^2(r(s, \psi)) ds, \quad (3)$$

where we sum over the channels, X , of neutralino pair annihilation, both monochromatic and continuum. The dN_γ^X/dE_γ are the photon energy spectra produced per annihilation event,

for each channel with partial annihilation cross section $\langle\sigma v\rangle_X$, which we may separate as

$$\sum_X \frac{dN_\gamma^X}{dE_\gamma} \langle\sigma v\rangle_X = 2v\sigma_{\gamma\gamma} \delta(E_\gamma - m_\chi) + v\sigma_{Z\gamma} \delta\left(E_\gamma - m_\chi\left(1 - \frac{M_Z^2}{4m_\chi^2}\right)\right) + \sum_i \frac{dN_{cont}^i}{dE_\gamma} \langle\sigma v\rangle_i. \quad (4)$$

The first and the second terms correspond to the monochromatic channels $\chi\chi \rightarrow 2\gamma/Z\gamma$, respectively, for which we use the one-loop annihilation cross sections $v\sigma_{\gamma\gamma}$ and $v\sigma_{Z\gamma}$ computed in [52, 53]. For the continuum component we calculate the dN_{cont}^i/dE_γ using the partial cross sections $\langle\sigma v\rangle_i$ for each of the two-body neutralino pair annihilation channels $i = \{q\bar{q}, \tau^+\tau^-, W^+W^-, ZZ, gg, Zh\}$, multiplied by the corresponding continuum spectra modelled using PYTHIA.

We follow the standard procedure [5] for the halo factor in (3), defining a dimensionless average halo factor as an integral along light-of-sight (los) directions within a solid angle $\Delta\Omega$:

$$\bar{J}(\Delta\Omega) \Delta\Omega \equiv \frac{1}{R_\odot \rho_\odot^2} \int_{\Delta\Omega} d\Omega \int_{\text{los}} \rho^2(r(s, \psi)) ds. \quad (5)$$

where R_\odot is the solar distance from the GC and ρ_\odot is local dark matter density. With these definitions, the prompt part in (3) takes the form

$$\left. \frac{d\Phi_\gamma(E_\gamma)}{dE_\gamma} \right|_{\text{prompt}} = \frac{R_\odot}{2\pi} \left(\frac{\rho_\odot}{2m_\chi} \right)^2 (\bar{J}(\Delta\Omega) \Delta\Omega) \sum_X \frac{dN_\gamma^X}{dE_\gamma} \langle\sigma v\rangle_X. \quad (6)$$

We use the values $R_\odot = 8.5$ kpc and $\rho_\odot = 0.3$ GeV/cm³. The integration along the light-of-sight direction can be performed using

$$r^2(s, \psi) = R_\odot^2 - 2sR_\odot \cos\psi + s^2, \quad (7)$$

where ψ is the angle with respect to the GC direction. Defining the function

$$J(\psi) \equiv \frac{1}{R_\odot \rho_\odot^2} \int_0^{s_{max}(\psi)} \rho^2(\sqrt{R_\odot^2 - 2sR_\odot \cos\psi + s^2}) ds, \quad (8)$$

one can calculate the halo average in a cone within angle ϕ , that defines the size of the observation window around the GC, as

$$\bar{J}(\Delta\Omega) \Delta\Omega = 2\pi \int_{\cos\phi}^1 J(\psi) d(\cos\psi). \quad (9)$$

This is the quantity introduced in (5), where we have used $\Delta\Omega = 2\pi(1 - \cos\phi)$. The upper limit s_{max} in (8) is calculated in terms of the Milky Way halo size R_{MW}

$$s_{max}(\psi) = \sqrt{R_{MW}^2 - (R_\odot \sin\psi)^2} + R_\odot \cos\psi \quad (10)$$

although, as noted in [54], the contribution of the integration beyond the scale radius $\sim 20 - 30$ kpc is negligible.

The behavior of the galactic DM halo, especially in the inner region, is a very controversial topic. Although some N-body simulations indicate that the halo presents a highly cusped behavior towards its center [36, 55], other simulations [39, 56] as well as atomic hydrogen HI observations on dwarf spiral galaxies [57] indicate shallower profiles. Recently, the Via Lactea 2 simulations [58] seem to support a cuspy profile like NFW, whereas the Aquarius DM simulation project [59] favors a different parameterization [38, 60], that does not have such a cuspy character in the inner region, such as the Einasto profile. This unsettled issue of the cuspiness has significant impact on the theoretical predictions for the γ -ray flux emitted from the GC, and suggests a substantial theoretical uncertainty in calculating this. To address this uncertainty, we study three halo profiles that behave differently in the inner region of the Milky Way: NFW [36], Einasto [37, 38] and a simple isothermal profile [39]. The NFW behaves like r^{-1} at small distances, while the Einasto and isothermal profiles are both non-singular towards the galactic center.

These profiles are defined by the density functions:

$$\begin{aligned}\rho_{\text{NFW}}(r) &= \rho_s \frac{r_s}{r} \left(1 + \frac{r}{r_s}\right)^{-2}, \\ \rho_{\text{Ein}}(r) &= \rho_s \exp\left[-\frac{2}{\alpha} \left(\left(\frac{r}{r_s}\right)^\alpha - 1\right)\right], \\ \rho_{\text{iso}}(r) &= \frac{\rho_s}{1 + (r/r'_s)^2}.\end{aligned}\tag{11}$$

We choose the following values of the model parameters: $r_s = 20$ kpc, $r'_s = 5$ kpc and $\alpha = 0.17$. The ρ_s parameter, which has a different numerical value for each profile, is defined in such a way that $\rho_\odot = \rho(R_\odot) = 0.3 \text{ GeV/cm}^3$. Assuming these numerical values, values of the halo factor $\bar{J}(\Delta\Omega) \Delta\Omega$ for three windows around the GC: 10, 7 and 5 degrees are tabulated in Table 1. The values in this Table are useful for understanding the relative sizes of the halo factor for the three halo profiles we study and the various windows. In the case of the the prompt component, the halo factor is simply multiplicative. In the case of the the ICS component, the halo factor is also, to a good approximation, multiplicative [47], but there are also other terms related to the photon background parameters and to the propagation of the lepton fluxes, etc., that are different for the various halo profiles and windows.

Model	10 deg	7 deg	5 deg
NFW	10.51	7.90	5.95
Einasto	19.68	15.21	11.56
Isothermal	1.21	0.62	0.32

Table 1: Values of the halo factor $\bar{J}(\Delta\Omega) \Delta\Omega$ for various galactic dark matter halo profiles and values of the angle ϕ that defines the size of the observation window around the GC.

3.1.2 The Inverse Compton Scattering component

Neutralino pair annihilation produces energetic electron and positron (e^\pm) fluxes mainly indirectly through the hadronization, fragmentation and decays of the primary annihilation products⁴. The indirectly produced e^\pm scatter on the ambient photon background, and through the ICS effect produce energetic photons. In order to calculate the ICS part we follow the tools and methods described in [10, 47].

The ICS flux is given by the equation

$$\begin{aligned} \left. \frac{d\Phi_\gamma(E_\gamma)}{dE_\gamma} \right|_{ICS} &= \frac{1}{E_\gamma^2} \frac{R_\odot}{2\pi} \left(\frac{\rho_\odot}{2m_\chi} \right)^2 \\ &\times \int_{\Delta\Omega} d\Omega \int_{m_e}^{m_\chi} dE_s \sum_i \frac{dN_{e^\pm}^i(E_s)}{dE} \langle \sigma v \rangle_i I_{IC}(E_\gamma, E_s, \psi), \end{aligned} \quad (12)$$

where E_s is the e^\pm injection energy and the halo function for the inverse Compton radiative process $I_{IC}(E_\gamma, E_s, \psi)$ is defined as

$$\begin{aligned} I_{IC}(E_\gamma, E_s, \psi) &= 2E_\gamma \int_{los} \frac{ds}{R_\odot} \left(\frac{\rho(r(s, \psi))}{\rho_\odot} \right)^2 \\ &\times \int_{m_e}^{E_s} dE \frac{\sum_a \mathcal{P}_{IC}^a(E_\gamma, E, r(s, \psi))}{b(E, r(s, \psi))} I(E, E_s, r(s, \psi)). \end{aligned} \quad (13)$$

We calculate the primary electron/positron fluxes $dN_{e^\pm}^i/dE$ produced by neutralino pair annihilation in the halo using `PYTHIA`, and the index i runs over the channels used for the photon prompt part. The functions \mathcal{P}_{IC}^a , the energy loss coefficient function $b(E, r)$ and the generalized halo function $I(E, E_s, r(s, \psi))$ are given in [47] and references therein.

The energy loss coefficient $b(E, r)$ depends on the profile of the magnetic field in the galactic plane, as described in [47, 61]. Recent estimates suggest that the magnitude of the magnetic field towards the GC can be larger by a factor of ten or more than in the solar

⁴The e^\pm fluxes produced directly through the channels $2\chi \rightarrow e^+e^-$ are negligible, because this process is P-wave suppressed and proportional to the small electron mass.

neighbourhood [62]. We have verified that a magnetic field that is stronger by a factor of 10 would result in a reduction of the ICS flux almost by a factor of two. This would affect the total γ -ray flux at low photon energy, where the ICS is dominant. However, since the most important part of the CMSSM γ signal is at higher energies, its effect on the global χ^2 that we calculate in the next Section is small, of the order of 10%. A similar remark applies to the possibility of energy losses due to interactions with gas in the GC [63].

The sum over the index a includes three photon backgrounds: the cosmic microwave background (CMB), the starlight in the galactic plane and the infrared radiation due to the rescattering of the starlight by dust. To calculate the ICS part, we follow the semi-analytic method described in [47], see also [10, 64], which yields results similar to numerical methods such as GALPROP [65]. In particular, for the e^\pm propagation parameters there are three commonly used models, called MIN, MED and MAX [64], that correspond to the minimal, median and maximal primary positron fluxes compatible with data on the boron to carbon ratio, B/C [66]. In this paper we choose the MED set of parameters, but we have checked that our findings do not depend significantly on this choice. Specifically, scanning through the various parameter sets, we find that the value of the ICS flux can be changed by at most 15%. In the low-energy range, this uncertainty affects analogously the total γ -ray signal, but its effect in the statistical χ^2 analysis in Section 4 is unnoticeable.

3.2 Examples within the CMSSM

Using the above treatments of the prompt and the ICS parts, we can evaluate the total flux in (1) and (2) at any point of the parameter space of the CMSSM. In Fig. 4, we display examples of the differential flux $E_\gamma^2 d\Phi_\gamma/dE_\gamma$ as a function of the photon energy E_γ in a 7-degree window around the GC. The blue curves are the prompt parts and the green curves correspond to the ICS contributions. We use the NFW profile in each case, and the four panels in Fig. 4 correspond to the four benchmark points C, E, L and M introduced in [31] and updated in [67]. These points belong to different characteristic regions of the CMSSM model that are cosmologically acceptable.

Referring to the left panel of Fig 1 for $\tan\beta = 10$, point C represents the low-mass region of the coannihilation strip for $\tan\beta = 10$ with $(m_{1/2}, m_0) = (400, 96)$ GeV, and point E is in the focus-point region with $(m_{1/2}, m_0) = (300, 2003)$ GeV (outside of the range shown in Fig 1a). Point L is in the coannihilation region at $(m_{1/2}, m_0) = (450, 312)$ GeV and $\tan\beta = 50$, and referring to the right panel of Fig 1 for large $\tan\beta$, point M is in the rapid-annihilation funnel region at large $(m_{1/2}, m_0) = (1075, 1045)$ GeV with $\tan\beta = 55$. The LSP

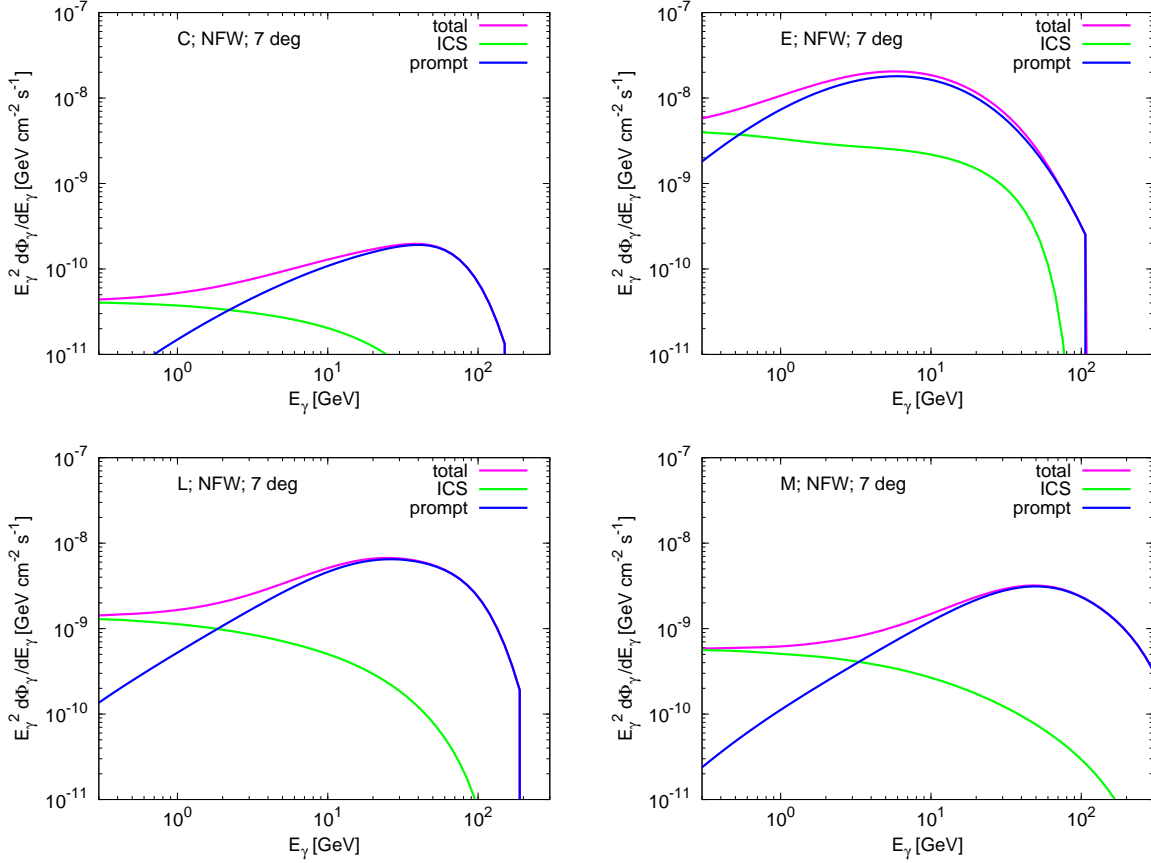


Figure 4: *The differential flux $E_\gamma^2 d\Phi_\gamma/dE_\gamma$ as a function of the photon energy E_γ for a 7 deg window around the GC. The blue curve is the prompt part and the green curve is the ICS flux. We use here the NFW profile, and the four panels correspond to the four benchmark CMSSM points C,E,L and M, which are described in the text.*

masses at the points C,E,L and M are $m_\chi = 165, 117, 193$ and 474 GeV, respectively. Since point C is in the coannihilation region, it has a small neutralino annihilation cross section, as we saw in Fig. 2, and hence the photon flux for point C is weaker than for the other benchmark points. The focus-point region point E has a stronger flux, because it has a larger annihilation cross section and small m_χ . The points L and M have comparable fluxes, but that of point M is relatively smaller, because there m_χ is larger ⁵.

In Fig. 5, we plot the fluxes $\Phi_\gamma(E_{th})$ in a 7-degree window around the GC, for the same benchmark points as functions of the threshold energy E_{th} , as defined in (2). Once again, the green curves represent the ICS parts, the cyan curves represent the monochromatic parts

⁵It is useful to note here that both the prompt and ICS fluxes are, in general, inversely proportional to m_χ^3 .

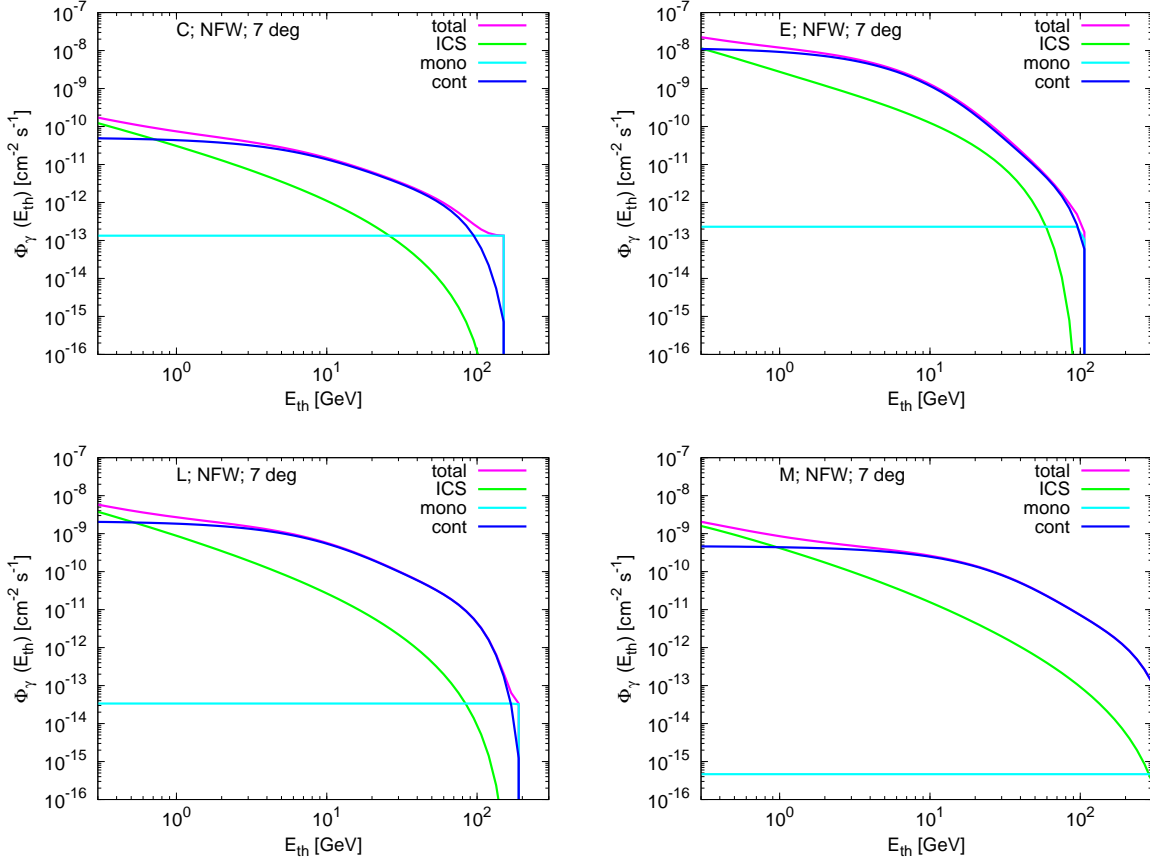


Figure 5: *The total flux $\Phi_\gamma(E_{th})$ as a function of the threshold energy E_{th} for a 7 deg window around the GC. The green curves represent the ICS part, the cyan curves represent the monochromatic part, and the blue curves the continuum part. We use here the NFW profile, and the four panels correspond to the four benchmark CMSSM points C, E, L and M, as in Fig. 4.*

and the blue curves the continuum parts. We see in these figures that the monochromatic component yields only a very small contribution in every case, as was discussed in the previous Section, and is also inversely proportional to m_χ^2 . Another remark concerns the relative magnitudes of the ICS and prompt components. Since the ICS component results from background photons energized by interaction with energetic charged leptons, it dominates for photon energies much smaller than m_χ . In particular, for LSP masses up to a few hundred GeV as along the benchmark strips we study, the ICS contribution becomes subdominant above the range $E_\gamma \gtrsim 1 - 3$ GeV, as can be seen in Fig. 4.

3.3 The background and Fermi-LAT data

The background has three main components: diffuse galactic emission (DGE), an isotropic extragalactic contribution and resolved point sources. DGE is produced essentially by the interaction of cosmic-ray nucleons and electrons with the interstellar medium. Nucleon interactions produce photons via π^0 decays, whereas electrons produce DGE via bremsstrahlung and ICS. For the determination of the DGE background component, a conventional model was developed [68] using the hypothesis that the cosmic-ray spectra in the Galaxy can be normalized to solar-system measurements. This model did not reproduce well the EGRET data, especially for $E_\gamma \sim \mathcal{O}(\text{GeV})$, resulting in the apparent EGRET excess [69]. An updated version of the model that was able to describe the data was developed in [70], and the recent Fermi-LAT measurements on the diffuse background component [12] are well reproduced by the updated version of the conventional model. This is the diffuse model that we use in our analysis. As was pointed out in [70], to estimate the errors in this model is a complicated task, but based on the quality of its fit to the data Fermi-LAT, we can say that is about 20% – 25% for photon energies up to 100 GeV.

The isotropic diffuse emission or isotropic gamma-ray background (IGRB) is much fainter and, although the term extragalactic gamma-ray background is usually applied, its extragalactic origin is not universally accepted. Various astrophysical objects can contribute to this emission, such as active galactic nuclei, galaxy clusters, blazars, star-forming galaxies, ultra-high-energy cosmic rays, etc. [71]. The Fermi-LAT collaboration measurement of the IGRB [15] is consistent with a power law, somewhat softer than the previous EGRET analogous measurement [72]. In any case, the isotropic component is subdominant in our analysis.

On the other hand, resolved point sources (RPS) provide an important part of the photon background from the direction of the GC. We use the first 11-month Fermi-LAT catalogue [14], which contains 1451 point sources modelled in the energy range 100 MeV to 100 GeV. The gamma flux of each point source is taken to obey a simple power law.

In order to evaluate the possible constraints imposed on the CMSSM parameter space by the latest Fermi-LAT data [13], we estimate the background using the Fermi-LAT Science Tools [73]. In our analysis, we use data collected by Fermi-LAT between Aug 4, 2008 and April 29, 2011, making a selection based on the recommendations of the collaboration. We focus our analysis in the energy range 300 MeV to 300 GeV, dividing it in 25 bins spaced evenly on a logarithmic scale. We have studied various windows around the GC in the range 1–10 degrees, but we choose as the basic region-of-interest (ROI) of our analysis the

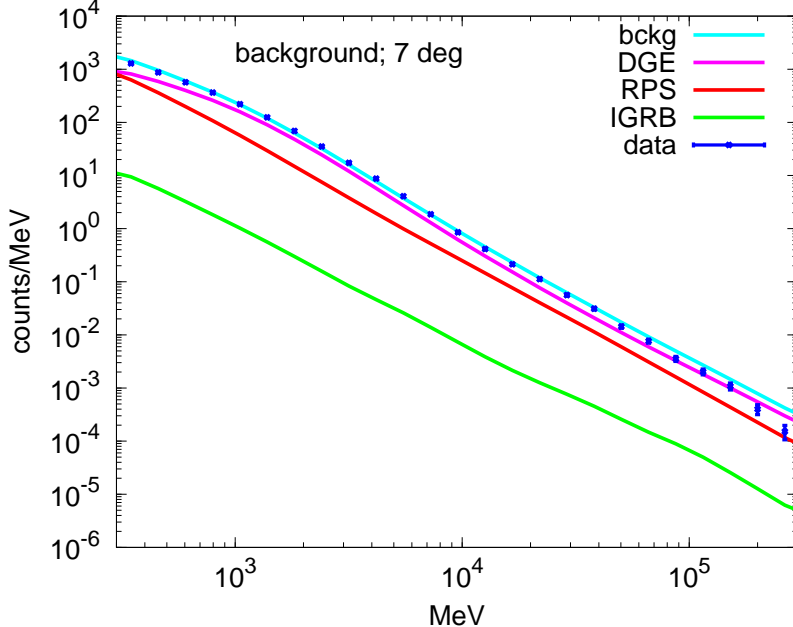


Figure 6: *The various background components in counts per MeV for a 7 deg window around the GC in the range 300 MeV to 300 GeV, estimated using the Fermi-LAT Science Tools [73]. We also display the Fermi-LAT data [13] collected during the period described in the text.*

7-degree window centered at the position of the brightest source in the GC: $RA = 266.46^{\circ}$, $Dec = -28.97^{\circ}$, as in [16]. Note however, that our conclusions are not overly sensitive to this choice of window size.

Fig. 6 displays the various background components obtained using the Science Tools [73], along with the data collected during the aforementioned period. The error bars attached to the data represent the purely statistical errors. We have performed a binned likelihood analysis using the `gtlike` tool, including in the background model file used in the fit 1) the galactic diffuse model, 2) the isotropic spectral template, and 3) the point sources, all as provided by the collaboration. Concerning the point sources, we have included additional RPS from the vicinity of the ROI, that possibly can contribute to the observed counts.

In Fig. 7 we plot the residuals in each of the 25 bins in the range 300 MeV to 300 GeV, i.e., the difference $(\text{counts} - \text{model})/\text{model}$, where in this case “model” includes just the background sources. As discussed earlier, the background models used to describe the collected data are able to reproduce them with an accuracy on the order of 25%, especially for photon energies up to 100 GeV. This was expected, since the background models are not adequate for energies larger than this [12, 14]. The shaded area represents the uncertainty in the effective area of the detector. As discussed in [16], the systematic uncertainty in the

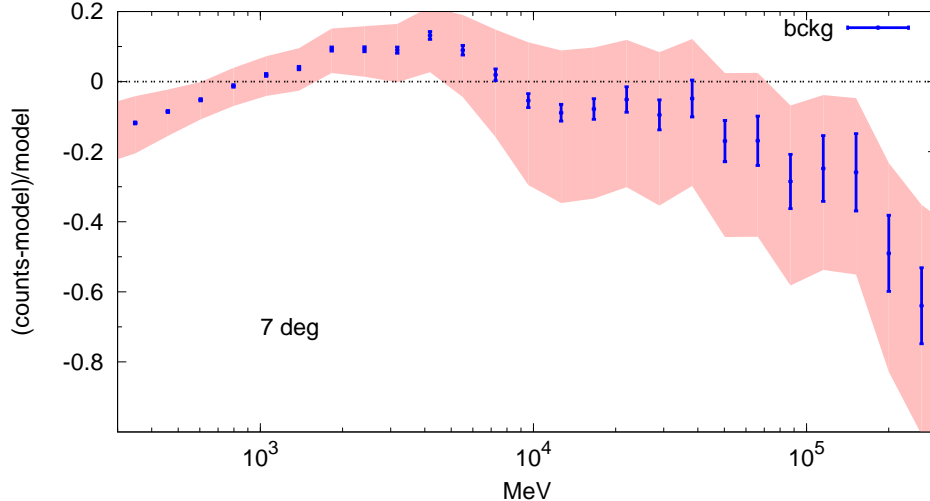


Figure 7: *The residuals in each bin of the available Fermi-LAT data [13] used in Fig. 6, for a 7 deg window around the GC in the range 300 MeV to 300 GeV, as compared to the estimated background model. The shaded area represents the uncertainty in the effective area of the detector as discussed in the text.*

effective area of the LAT is currently estimated as 10% at 100 MeV, decreasing to 5% at 560 MeV, and then increasing to 20% at 10 GeV. As suggested by in [16], we assume that this uncertainty propagates to the model predictions. With the systematic uncertainty included, we find $\chi^2 = 31.1$ for 25 degrees of freedom, corresponding to a p-value of 19%.

4 Experimental Perspectives

Using the results of the previous Section, we now compare the signals expected in CMSSM scenarios with the background, under various hypotheses, again using 25 logarithmic bins in the range 300 MeV to 300 GeV. We define the χ^2 function as

$$\chi^2 = \sum_{i=1}^{25} \frac{(d_i - (b_i + s_i))^2}{\sigma_i^2}, \quad (14)$$

where d_i is the number of the data counts per bin, b_i is the expected background as calculated by Science Tools [73], and s_i is the signal due to the dark matter halo for the corresponding bin. For the uncertainty, we have included both the statistical uncertainty in the data count as well as the systematic uncertainty in the effective area, σ_{ea} . These have been added in quadrature, so that $\sigma_i^2 = d_i + \sigma_{ea}^2$. In Fig. 8, we present the current Fermi-LAT data set [13] as blue dots with statistical error bars, the background estimate (red curve) and with the

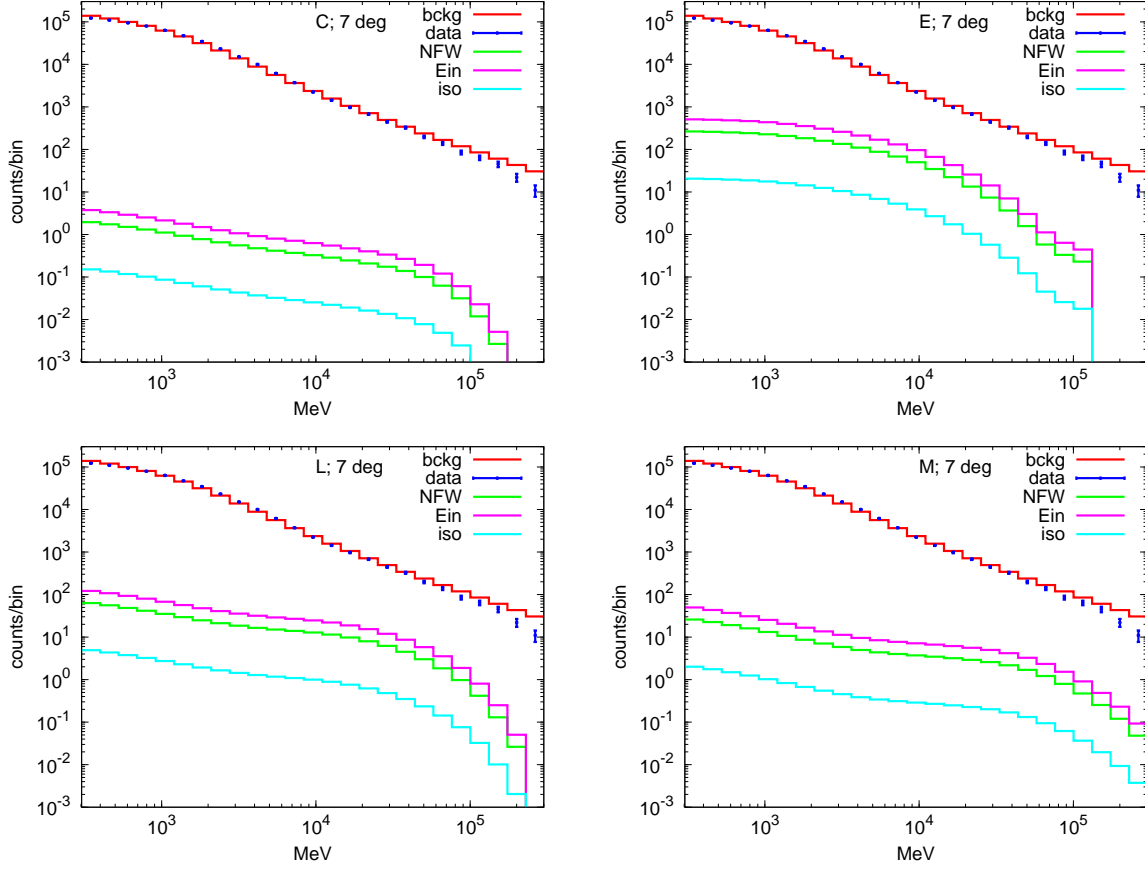


Figure 8: *The current Fermi-LAT data set [13], in counts per bin, as a function of photon energy E_γ in MeV, including the statistical error (blue points) for a 7-degree window around the GC. The red line is the corresponding estimated background. We also display the signals expected for the three halo profiles we are using: NFW, Einasto and isothermal and the four panels correspond to the four benchmark CMSSM points C, E, L and M, as in Fig. 4.*

signal corresponding to the three DM halo profiles discussed previously: NFW (green), Einasto (purple) and simple isothermal (cyan). The four panels of these figures correspond to the four CMSSM benchmark points C, E, L, M discussed in the previous Section, so the relative sizes of the signal can easily be understood. The coannihilation point C produces the weakest signal, as expected, and the focus-point benchmark E gives the strongest signal. Points L and M yield signals that are almost comparable, again as expected from Fig. 4. Had we chosen a point from the right side of the funnel, the signal would have been about a factor of 2 higher than shown for point M.

We start with a nominal implementation of the current experimental situation, that uses the present Fermi-LAT data set [13], assumes the current understanding of the background

and systematic errors, and uses an NFW density profile. As a preliminary to examining the signals along the WMAP strips shown in Fig. 1, we first consider a more global view across an $(m_{1/2}, m_0)$ plane in the CMSSM. As described in the previous section, in the absence of any supersymmetric contribution, our modeling of the astrophysical background give a value of $\chi^2 = 31.1$ for 25 degrees of freedom. In Fig. 9, we show for illustration (in yellow) contours of constant $\Delta\chi^2$ across the CMSSM $(m_{1/2}, m_0)$ plane for $\tan\beta = 55$ ⁶, exhibiting contours of $\Delta\chi^2 = 0, 1$ and 4 relative to the value of χ^2 without supersymmetry⁷. Note that there is a small region at low $m_{1/2}$, in the region already excluded by $b \rightarrow s\gamma$, where there is a small but insignificant improvement to χ^2 . As one can see in the left panel of Fig. 9, where an NFW profile has been assumed, a modest constraint is imposed by the present Fermi data. In addition to the area at small $m_{1/2}$ that is already excluded by supersymmetry searches at LEP, the $\Delta\chi^2 = 1$ contour runs between the branches of the rapid-annihilation funnel, and disfavours the right branch at the 68% CL. The $\Delta\chi^2 = 4$ contour runs deep inside the funnel where the relic density is below the WMAP range. In the right panel, where the Einasto profile has been assumed, the disfavoured region is somewhat larger, as expected from the values of the halo factors in the Table 1. On the other hand, based on these values, the opposite is expected for the for the isothermal model.

We now focus on the WMAP strips for $\tan\beta = 10$ and 55. The results of our nominal implementation of the current and possible future Fermi constraints are shown in Fig. 10 for the coannihilation and funnel strips (upper panels) and $\tan\beta = 10$ (left panels) and $\tan\beta = 55$ (right panels). As a function of $m_{1/2}$ along each of these lines, we display the χ^2 function for the background alone, which is a constant 31.1 for 25 degrees of freedom, and the corresponding χ^2 function for the combination of the background with the signal calculated as a function of $m_{1/2}$ in each scenario, for the current Fermi-LAT data [13]. Also shown are the possible results from future 5- and 10-year data sets. The baseline χ^2 is correspondingly higher due to the expected improvement in the statistical uncertainty in the data, assuming no improvement in the systematic uncertainty associated with the effective area. The horizontal lines assuming no supersymmetry are not shown for these hypothetical

⁶We do not show analogous results for $\tan\beta = 10$, since the results are unpromising, as we see below when we restrict our attention to the WMAP strips.

⁷We recall that the relic LSP density is too large in the interior of the plane between the WMAP strips, and too small in the outer regions between the WMAP strips and the charged-LSP and electroweak symmetry breaking boundaries. The interior region is forbidden in the R -conserving scenario discussed here, whereas the outer regions could be acceptable in the presence of some other component of dark matter. However, in this case the annihilation rate should be reduced by the square of the relic LSP density relative to the WMAP dark matter density. Only the intersections of the $\Delta\chi^2$ contours with the WMAP strips should be taken literally.

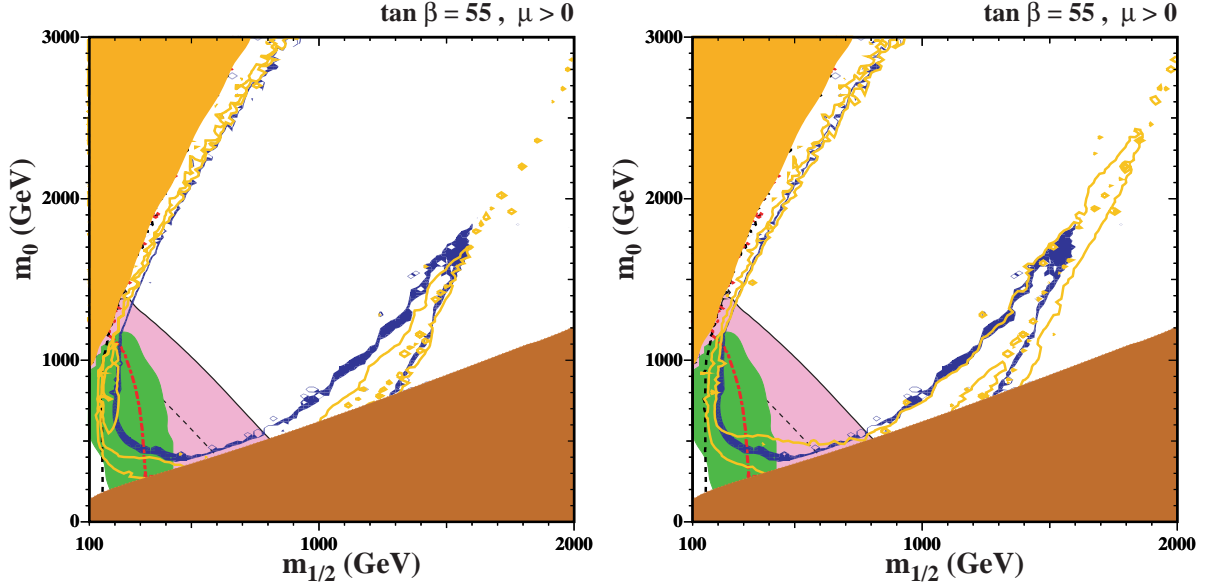


Figure 9: *Contours of $\Delta\chi^2 = 0, 1, 4$ in the $m_{1/2}, m_0$ plane for $\tan\beta = 55$ (shown in yellow). In the left panel, we assume an NFW profile for dark matter in the core of the galaxy, whereas in the right panel we assume an Einasto profile. Conventions for the other curves and shaded regions are as for Fig. 1.*

data sets. In each case, the results assuming an NFW profile are shown as solid lines, and results assuming an Einasto profile are shown as dashed lines.

We see immediately that the calculated signal with the current Fermi-LAT data set [13] has very little effect on the overall χ^2 function along the coannihilation strip for $\tan\beta = 10$ (upper left panel), whereas somewhat larger effects are visible along the WMAP strips shown in the other panels. However, in all cases except along the second funnel strip for $\tan\beta = 55$ the change in the χ^2 function is < 1 in the case of the NFW profile (solid blue lines), and hence not significant. In general, adding the supersymmetric signal worsens slightly the quality of the fit, though there is a slight improvement along the focus-point strip for $\tan\beta = 10$ for $200 \text{ GeV} < m_{1/2} < 400 \text{ GeV}$. The (red) dashed curves in Fig. 10 show the resulting χ^2 functions assuming an Einasto dark matter profile. While this does yield somewhat larger effects, we see that $\Delta\chi^2 \lesssim 3$ even along the right branch of the funnel for $\tan\beta = 55$, and a 95% CL exclusion is not possible.

Hence, the most that one could hope for along most of the WMAP strips studied is some inconclusive level of disfavour, except in the limited region of small $m_{1/2}$ for $\tan\beta = 10$ where some improvement in the overall χ^2 of a global fit might eventually be possible. Significant

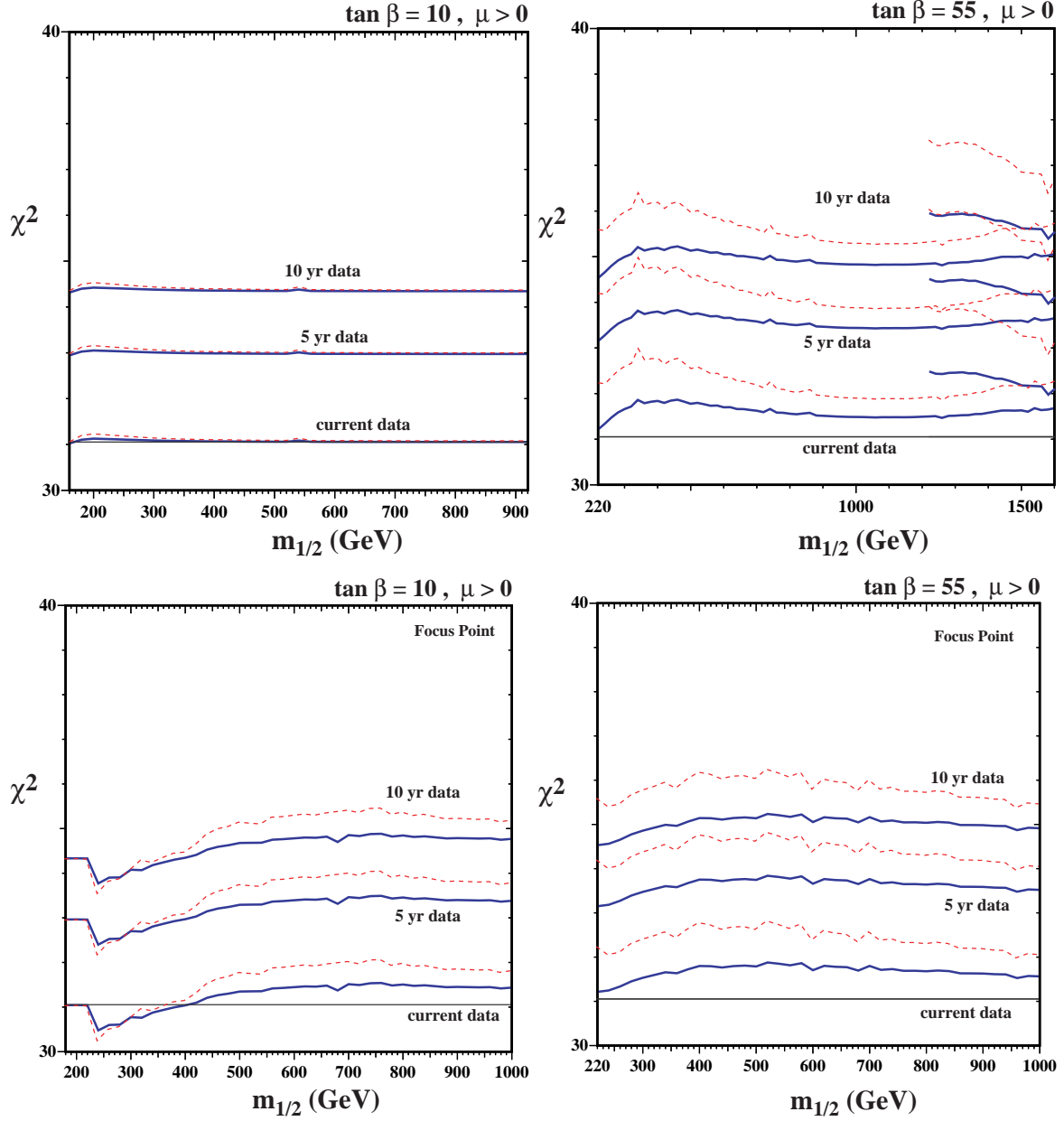


Figure 10: The χ^2 functions along the CMSSM WMAP strips as functions of $m_{1/2}$ for $\tan \beta = 10$ (left panels) and $\tan \beta = 55$ (right panels), in the coannihilation and funnel regions (upper panels) and in the focus-point region (lower panels). In each panel, we display the χ^2 function for the background alone, a horizontal line at $\chi^2 = 31.1$, and the χ^2 function obtained by adding the calculated $\chi - \chi$ annihilation signal in the current (approximately 2 $1/2$ year) Fermi data sample and in projected 5- and 10-year data sets. Solid (blue) curves are based on an NFW profile, while dashed (red) curves are based on an Einasto profile.

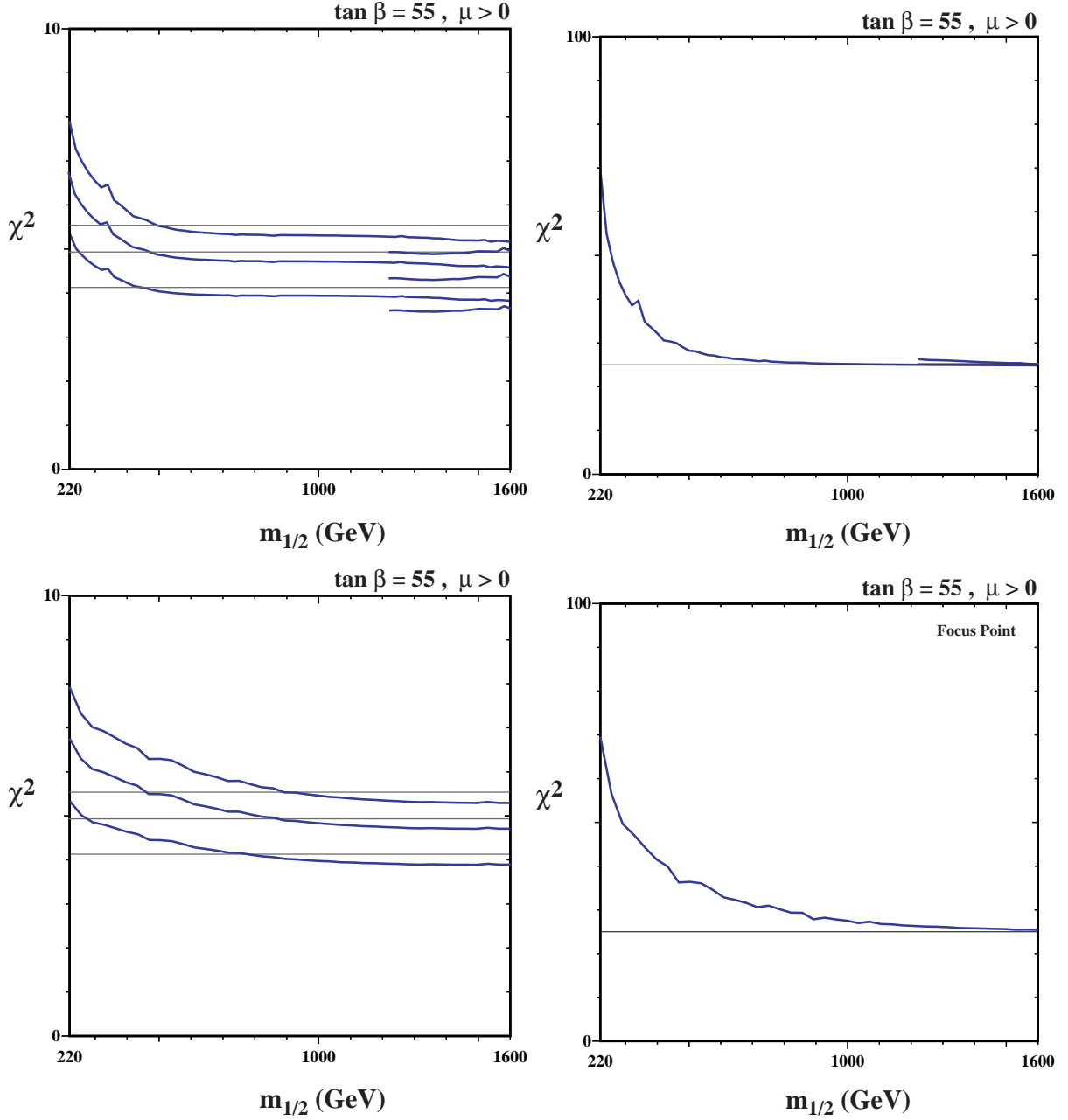


Figure 11: The χ^2 functions as functions of $m_{1/2}$ along the CMSSM focus-point WMAP strip for $\tan \beta = 55$ assuming a factor of 2, 3 or 4 reduction in the systematic error σ_{ea}^2 (left panels) or a negligible systematic error (right panels), assuming in all cases that an improved estimate of the background brings it to $\pm 1\sigma$ from the data. The upper (lower) panels are for the coannihilation/funnel strip (focus-point strip).

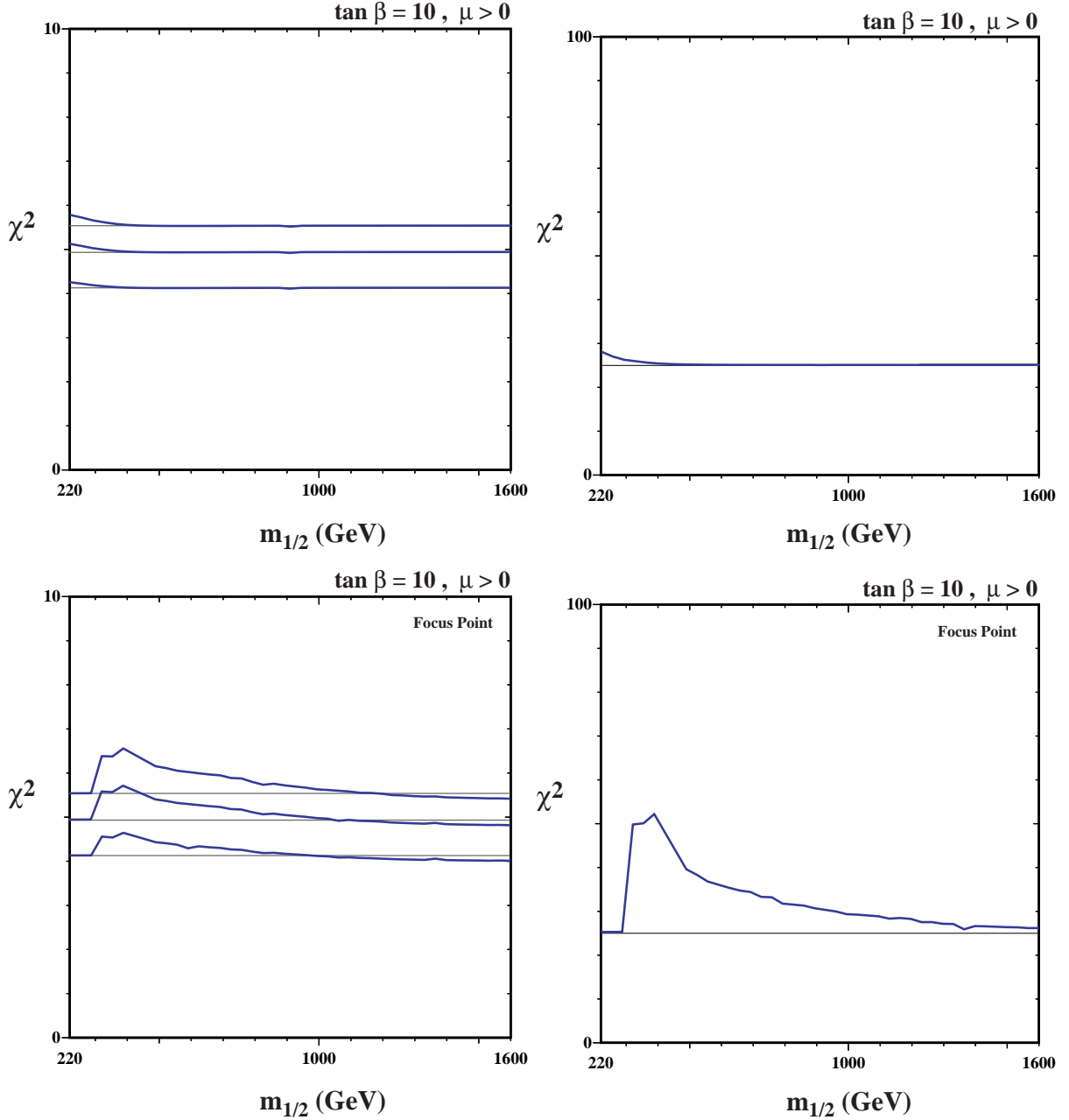


Figure 12: *As in Fig. 11, but for $\tan \beta = 10$.*

improvements in our current understandings of the background and/or systematic errors would be required before the scenarios studied could be constrained significantly.

Examples of the effects of possible improvements in understanding the background and systematic errors are shown in Fig. 11, in the cases of the coannihilation/funnel strip (upper

panels) and focus-point strip (lower panels) WMAP strips with $\tan\beta = 55$, assuming an NFW profile. The χ^2 functions in the absence of any supersymmetric signal are shown as horizontal black lines, and the effects of including a signal are shown as blue lines. In all of these panels, we have assumed that improvements to our understanding of the background bring it to lie within 1σ of the data, with the sign of the discrepancy chosen randomly in each bin. In the left panels, we also assume reductions in the current systematic error in the effective area by a factors of 2, 3 and 4 in σ_{ea}^2 , whereas in the right panels the systematic error is assumed to be negligible⁸. We see immediately in the left panels that reducing the systematic error by a factor of 2 does not improve greatly the discrimination between the background-only and signal + background hypotheses. Even a reduction by a factor of 4 does not lead to a 95% CL exclusion limit, whereas we see in the right panels that a reduction in the systematic error to a negligible level might provide such discrimination. Depending on the evolution of the understanding of the background, adding a CMSSM might affect significantly the fit for small $m_{1/2}$. With the present background estimate, 5 or 10 years of Fermi data might provide evidence for the CMSSM at small $m_{1/2}$, albeit in the region disfavoured by $b \rightarrow s\gamma$, or possibly evidence against the CMSSM in the region $m_{1/2} > 500$ GeV where accelerator constraints are currently irrelevant. The corresponding figures for $\tan\beta = 10$ with improved systematics are shown in Fig. 12. In the case of the coannihilation strip for $\tan\beta = 10$, even the absence of systematic errors would not allow significant information to be obtained, though some information might be obtainable about the focus-point strip. For instance, using the Einasto profile instead of NFW, the χ^2 of the last panel in the Fig. 12 is about 3 times bigger, enabling more definite conclusions to be drawn.

5 Summary and Prospects

We have studied in this paper the potential of searches by the Fermi-LAT detector [13] for γ rays from the Galactic centre produced by the annihilations of neutralino LSPs in the CMSSM. We have shown predictions for benchmark points, $(m_{1/2}, m_0)$ planes, and the concentrated on the WMAP strips for $\tan\beta = 10$ and 55. We have found that the γ -ray signal would be very difficult to detect along the coannihilation strip for $\tan\beta = 10$, as expected from the relatively small $\chi\chi$ annihilation cross section along this strip. The focus-

⁸For large m_χ even a small signal improves slightly the fit, in comparison to the background case only. So we see the χ^2 of the signal is smaller than the χ^2 of the background for large $m_{1/2}$. This improvement, for the case of the reduced systematic error, is due to the χ^2 contribution of the last bins that contain energetic photons with $E_\gamma > 150$ GeV.

point strip for $\tan\beta = 10$ and both the coannihilation/funnel and focus-point strips for $\tan\beta = 55$ have larger annihilation cross sections and offer better prospects, though even in these cases the present data do not offer good prospects for discriminating between models, because of uncertainties in the background estimates and the current systematic errors of the Fermi-LAT detector.

Future Fermi-LAT data sets might offer some information about parameters of the CMSSM, also in regions of parameter space not accessible to accelerator experiments. However, this would require several more years of data and a substantial reduction in the present systematic error. This is therefore a priority for optimizing the prospects for future Fermi-LAT constraints on the CMSSM from searches for γ rays from the Galactic centre. Quantitative understanding of the constraints imposed by Fermi-LAT results would also require advances in our understanding of the dark matter density profile in the core of the Galaxy, since we see considerable differences between results assuming NFW and Einasto profiles.

The Fermi-LAT detector also has data on γ rays from many other astrophysical sources, including the Galactic bulge, dwarf galaxies and diffuse emissions. We therefore plan to extend our analysis to these cases. However, it is clear that it will always be more difficult to pin down the CMSSM than some other supersymmetric models via searches for energetic γ rays from astrophysical sources, and the same remark applies to other astrophysical strategies to look for neutralino annihilations.

Acknowledgements

The work of J.E. was supported partly by the London Centre for Terauniverse Studies (LCTS), using funding from the European Research Council via the Advanced Investigator Grant 267352. The work of K.A.O. was supported in part by DOE grant DE-FG02-94ER-40823 at the University of Minnesota. K.A.O. also thanks SLAC (supported by the DOE under contract number DE-AC02-76SF00515) and the Stanford Institute for Theoretical Physics for their hospitality and support. The work of V.C.S. was supported by Marie Curie International Reintegration grant SUSYDM-PHEN, MIRG-CT-2007-203189. We acknowledge contributions by Yudi Santoso in the early stages of this work. We thank Elliott Bloom, Aldo Morselli, Simona Murgia and Stefano Profumo for helpful discussions about Fermi-LAT data. V.C.S. thanks Johann Cohen-Tanugi, Marco Cirelli and Catena Riccardo for useful discussions.

References

- [1] J. R. Ellis, J. S. Hagelin, D. V. Nanopoulos, K. A. Olive and M. Srednicki, Nucl. Phys. B **238**, 453 (1984); see also H. Goldberg, Phys. Rev. Lett. **50**, 1419 (1983).
- [2] J. Silk and M. Srednicki, Phys. Rev. Lett. **53** (1984) 624; F. W. Stecker, S. Rudaz, and T.F. Walsh, Phys. Rev. Lett. **55** (1985) 2622; M. Srednicki, S. Theissen and J. Silk, Phys. Rev. Lett. **56** (1986) 263; S. Rudaz, Phys. Rev. Lett. **56** (1986) 2188; S. Rudaz and F. Stecker, Ap.J., **325** (1988) 16; J. Ellis, R. A. Flores, K. Freese, S. Ritz, D. Seckel and J. Silk, Phys. Lett. **B214** (1989) 403; F. Stecker and A. Tylka, Ap.J. **343** (1989) 169; L. Bergstrom, L. and H. Snellman, Phys. Rev. **D37** (1988) 3737; S. Rudaz, Phys. Rev. **D39** (1989) 3549; A. Bouquet, P. Salati and J. Silk, Phys. Rev. **D40** (1989) 3168; G.F. Giudice and K. Greist, Phys. Rev. **D40** (1989) 2549; L. Bergstrom, Phys. Lett. **B225** (1989) 372. S. Rudaz and F. Stecker, Ap.J. **368** (1991) 406.
- [3] L. Bergstrom, J. Edsjo and C. Gunnarsson, Phys. Rev. D **63**, 083515 (2001) [arXiv:astro-ph/0012346]; L. Bergstrom, J. Edsjo and P. Ullio, Phys. Rev. Lett. **87**, 251301 (2001) [arXiv:astro-ph/0105048]; W. de Boer, M. Herold, C. Sander and V. Zhukov, Eur. Phys. J. C **33**, S981 (2004) [arXiv:hep-ph/0312037]; N. Fornengo, L. Pieri and S. Scopel, Phys. Rev. D **70**, 103529 (2004) [arXiv:hep-ph/0407342]; D. Hooper and P. D. Serpico, JCAP **0706**, 013 (2007) [arXiv:astro-ph/0702328]; S. Dodelson, A. V. Belikov, D. Hooper and P. Serpico, Phys. Rev. D **80**, 083504 (2009) [arXiv:0903.2829 [astro-ph.CO]]; L. Bergstrom, T. Bringmann and J. Edsjo, Phys. Rev. D **83**, 045024 (2011) [arXiv:1011.4514 [hep-ph]]; E. J. Baxter and S. Dodelson, arXiv:1103.5779 [astro-ph.CO].
- [4] T. Bringmann, L. Bergstrom, J. Edsjo, JHEP **0801** (2008) 049 [arXiv:0710.3169 [hep-ph]].
- [5] L. Bergstrom, P. Ullio, J. H. Buckley, Astropart. Phys. **9** (1998) 137-162 [astro-ph/9712318], P. Ullio, L. Bergstrom, J. Edsjo, C. G. Lacey, Phys. Rev. **D66** (2002) 123502 [astro-ph/0207125], Y. Mambrini, C. Munoz, Astropart. Phys. **24** (2005) 208-230 [arXiv:hep-ph/0407158 [hep-ph]].
- [6] V. Berezhinsky, A. Bottino and G. Mignola, Phys. Lett. B **325**, 136 (1994) [arXiv:hep-ph/9402215]; A. Cesarini, F. Fucito, A. Lionetto, A. Morselli and P. Ullio, Astropart. Phys. **21**, 267 (2004) [arXiv:astro-ph/0305075]; S. Dodelson, D. Hooper and

- P. D. Serpico, Phys. Rev. D **77**, 063512 (2008) [arXiv:0711.4621 [astro-ph]]; P. D. Serpico and D. Hooper, New J. Phys. **11**, 105010 (2009) [arXiv:0902.2539 [hep-ph]]; R. M. Crocker, N. F. Bell, C. Balazs and D. I. Jones, Phys. Rev. D **81**, 063516 (2010) [arXiv:1002.0229 [hep-ph]].
- [7] P. Gondolo and J. Silk, Phys. Rev. Lett. **83**, 1719 (1999) [arXiv:astro-ph/9906391]; P. Ullio, H. Zhao and M. Kamionkowski, Phys. Rev. D **64** (2001) 043504 [arXiv:astro-ph/0101481]; D. Merritt, M. Milosavljevic, L. Verde and R. Jimenez, Phys. Rev. Lett. **88** (2002) 191301 [arXiv:astro-ph/0201376]; G. Bertone, G. Sigl and J. Silk, Mon. Not. Roy. Astron. Soc. **337**, 98 (2002) [arXiv:astro-ph/0203488]; R. Aloisio, P. Blasi and A. V. Olinto, JCAP **0405**, 007 (2004) [arXiv:astro-ph/0402588]; G. Bertone and D. Merritt, Phys. Rev. D **72** (2005) 103502 [arXiv:astro-ph/0501555]; H. S. Zhao and J. Silk, Phys. Rev. Lett. **95** (2005) 011301 [arXiv:astro-ph/0501625]; M. Regis and P. Ullio, Phys. Rev. D **78**, 043505 (2008) [arXiv:0802.0234 [hep-ph]].
- [8] N. W. Evans, F. Ferrer and S. Sarkar, Phys. Rev. D **69**, 123501 (2004) [arXiv:astro-ph/0311145]; S. Colafrancesco, S. Profumo and P. Ullio, Phys. Rev. D **75**, 023513 (2007) [arXiv:astro-ph/0607073]; P. Scott, J. Conrad, J. Edsjo, L. Bergstrom, C. Farnier and Y. Akrami, JCAP **1001**, 031 (2010) [arXiv:0909.3300 [astro-ph.CO]]; E. J. Baxter, S. Dodelson, S. M. Koushiappas and L. E. Strigari, Phys. Rev. D **82**, 123511 (2010) [arXiv:1006.2399 [astro-ph.GA]].
- [9] Y. Mambrini, C. Munoz and E. Nezri, JCAP **0612**, 003 (2006) [arXiv:hep-ph/0607266]; E. A. Baltz *et al.*, JCAP **0807**, 013 (2008) [arXiv:0806.2911 [astro-ph]]; K. N. Abazajian, P. Agrawal, Z. Chacko and C. Kilic, JCAP **1011**, 041 (2010) [arXiv:1002.3820 [astro-ph.HE]]; D. T. Cumberbatch, Y. L. Tsai and L. Roszkowski, Phys. Rev. D **82**, 103521 (2010) [arXiv:1003.2808 [astro-ph.HE]]; G. Vertongen and C. Weniger, arXiv:1101.2610 [hep-ph].
- [10] N. Bernal and S. Palomares-Ruiz, arXiv:1006.0477 [astro-ph.HE].
- [11] J. L. Feng, K. T. Matchev and F. Wilczek, Phys. Rev. D **63**, 045024 (2001) [arXiv:astro-ph/0008115]; J. R. Ellis, J. L. Feng, A. Ferstl, K. T. Matchev and K. A. Olive, Eur. Phys. J. C **24**, 311 (2002) [arXiv:astro-ph/0110225]. H. Baer and J. O’Farrill, JCAP **0404**, 005 (2004) [arXiv:hep-ph/0312350] A. Bottino, F. Donato, N. Fornengo and S. Scopel, Phys. Rev. D **70**, 015005 (2004) [arXiv:hep-ph/0401186]; H. Baer, A. Belyaev, T. Krupovnickas and J. O’Farrill, JCAP **0408**, 005 (2004)

- [arXiv:hep-ph/0405210]; Y. Mambrini and C. Munoz, JCAP **0410**, 003 (2004) [arXiv:hep-ph/0407352]; H. Baer, A. Mustafayev, S. Profumo, A. Belyaev and X. Tata, JHEP **0507**, 065 (2005) [arXiv:hep-ph/0504001]; Y. Mambrini and E. Nezri, Eur. Phys. J. C **50**, 949 (2007) [arXiv:hep-ph/0507263] Y. Mambrini, C. Munoz, E. Nezri and F. Prada, AIP Conf. Proc. **805**, 475 (2006) [arXiv:hep-ph/0509300]; S. Profumo, arXiv:1105.5162 [hep-ph].
- [12] A. A. Abdo *et al.* [Fermi LAT Collaboration], Astrophys. J. **703** (2009) 1249 [arXiv:0908.1171 [astro-ph.HE]]; A. A. Abdo *et al.* [Fermi LAT Collaboration], Phys. Rev. Lett. **103** (2009) 251101 [arXiv:0912.0973 [astro-ph.HE]].
- [13] A. A. Abdo *et al.*, Astrophys. J. **712**, 147 (2010) [arXiv:1001.4531 [astro-ph.CO]]; A. A. Abdo *et al.*, Phys. Rev. Lett. **104**, 091302 (2010) [arXiv:1001.4836 [astro-ph.HE]]; A. A. Abdo *et al.* [Fermi-LAT Collaboration], JCAP **1004**, 014 (2010) [arXiv:1002.4415 [astro-ph.CO]].
- [14] A. A. Abdo *et al.* [The Fermi-LAT collaboration], Astrophys. J. Suppl. **188** (2010) 405 [arXiv:1002.2280 [astro-ph.HE]].
- [15] A. A. Abdo *et al.* [The Fermi-LAT collaboration], Phys. Rev. Lett. **104** (2010) 101101 [arXiv:1002.3603 [astro-ph.HE]].
- [16] V. Vitale and A. Morselli, for the Fermi-LAT Collaboration, arXiv:0912.3828 [astro-ph.HE].
- [17] V.A. Acciari *et al.* [The VERITAS Collaboration], Astrophys. J. **720**, 1174 (2010) [arXiv:1006.5955 [astro-ph.CO]].
- [18] J. Aleksic *et al.* [The MAGIC Collaboration], arXiv:1103.0477 [astro-ph].
- [19] A. Abramowski *et al.* [H.E.S.S. Collaboration], Phys. Rev. Lett. **106**, 161301 (2011) [arXiv:1103.3266 [astro-ph.HE]].
- [20] D. Hooper and L. Goodenough, Phys. Lett. B **697**, 412 (2011) [arXiv:1010.2752 [hep-ph]].
- [21] M. Drees and M. M. Nojiri, Phys. Rev. D **47**, 376 (1993)[arXiv:hep-ph/9207234]; H. Baer and M. Brhlik, Phys. Rev. D **53**, 597 (1996) [arXiv:hep-ph/9508321] and Phys. Rev. D **57**, 567 (1998) [arXiv:hep-ph/9706509]; H. Baer, M. Brhlik, M. A. Diaz, J. Ferrandis, P. Mercadante, P. Quintana and X. Tata, Phys. Rev. D **63** (2001) 015007

- [arXiv:hep-ph/0005027]; A. B. Lahanas, D. V. Nanopoulos and V. C. Spanos, *Mod. Phys. Lett. A* **16** (2001) 1229 [arXiv:hep-ph/0009065]; A. B. Lahanas and V. C. Spanos, *Eur. Phys. J. C* **23** (2002) 185 [arXiv:hep-ph/0106345].
- [22] J. R. Ellis, T. Falk, K. A. Olive and M. Schmitt, *Phys. Lett. B* **388** (1996) 97 [arXiv:hep-ph/9607292]; *Phys. Lett. B* **413** (1997) 355 [arXiv:hep-ph/9705444]; J. R. Ellis, T. Falk, G. Ganis, K. A. Olive and M. Schmitt, *Phys. Rev. D* **58** (1998) 095002 [arXiv:hep-ph/9801445]; V. D. Barger and C. Kao, *Phys. Rev. D* **57** (1998) 3131 [arXiv:hep-ph/9704403]. J. R. Ellis, T. Falk, G. Ganis and K. A. Olive, *Phys. Rev. D* **62** (2000) 075010 [arXiv:hep-ph/0004169].
- [23] J. R. Ellis, T. Falk, G. Ganis, K. A. Olive and M. Srednicki, *Phys. Lett. B* **510** (2001) 236 [arXiv:hep-ph/0102098].
- [24] V. D. Barger and C. Kao, *Phys. Lett. B* **518** (2001) 117 [arXiv:hep-ph/0106189]; L. Roszkowski, R. Ruiz de Austri and T. Nihei, *JHEP* **0108** (2001) 024 [arXiv:hep-ph/0106334]; A. Djouadi, M. Drees and J. L. Kneur, *JHEP* **0108** (2001) 055 [arXiv:hep-ph/0107316]; U. Chattopadhyay, A. Corsetti and P. Nath, *Phys. Rev. D* **66** (2002) 035003 [arXiv:hep-ph/0201001]; J. R. Ellis, K. A. Olive and Y. Santoso, *New Jour. Phys.* **4** (2002) 32 [arXiv:hep-ph/0202110]; H. Baer, C. Balazs, A. Belyaev, J. K. Mizukoshi, X. Tata and Y. Wang, *JHEP* **0207** (2002) 050 [arXiv:hep-ph/0205325]; R. L. Arnowitt and B. Dutta, arXiv:hep-ph/0211417.
- [25] J. R. Ellis, K. A. Olive, Y. Santoso and V. C. Spanos, *Phys. Lett. B* **565** (2003) 176 [arXiv:hep-ph/0303043].
- [26] H. Baer and C. Balazs, *JCAP* **0305**, 006 (2003) [arXiv:hep-ph/0303114]; A. B. Lahanas and D. V. Nanopoulos, *Phys. Lett. B* **568**, 55 (2003) [arXiv:hep-ph/0303130]; U. Chattopadhyay, A. Corsetti and P. Nath, *Phys. Rev. D* **68**, 035005 (2003) [arXiv:hep-ph/0303201]; C. Muñoz, *Int. J. Mod. Phys. A* **19**, 3093 (2004) [arXiv:hep-ph/0309346].
- [27] [The Muon $g-2$ Collaboration], *Phys. Rev. Lett.* **92** (2004) 161802, [arXiv:hep-ex/0401008]; G. Bennett et al. [The Muon $g-2$ Collaboration], *Phys. Rev. D* **73** (2006) 072003 [arXiv:hep-ex/0602035].
- [28] D. Stockinger, *J. Phys. G* **34** (2007) R45 [arXiv:hep-ph/0609168]; J. Miller, E. de Rafael and B. Roberts, *Rept. Prog. Phys.* **70** (2007) 795 [arXiv:hep-ph/0703049]; J. Prades,

- E. de Rafael and A. Vainshtein, arXiv:0901.0306 [hep-ph]; F. Jegerlehner and A. Nyfeler, Phys. Rept. **477**, 1 (2009) [arXiv:0902.3360 [hep-ph]]; M. Davier, A. Hoecker, B. Malaescu, C. Z. Yuan and Z. Zhang, Eur. Phys. J. C **66**, 1 (2010) [arXiv:0908.4300 [hep-ph]]. J. Prades, Acta Phys. Polon. Supp. **3**, 75 (2010) [arXiv:0909.2546 [hep-ph]]; T. Teubner, K. Hagiwara, R. Liao, A. D. Martin and D. Nomura, arXiv:1001.5401 [hep-ph]; M. Davier, A. Hoecker, B. Malaescu and Z. Zhang, arXiv:1010.4180 [hep-ph].
- [29] S. Chen *et al.* [CLEO Collaboration], Phys. Rev. Lett. **87** (2001) 251807 [arXiv:hep-ex/0108032]; P. Koppenburg *et al.* [Belle Collaboration], Phys. Rev. Lett. **93** (2004) 061803 [arXiv:hep-ex/0403004]. B. Aubert *et al.* [BaBar Collaboration], arXiv:hep-ex/0207076; E. Barberio *et al.* [Heavy Flavor Averaging Group (HFAG)], arXiv:hep-ex/0603003.
- [30] E. Komatsu *et al.* [WMAP Collaboration], Astrophys. J. Suppl. **192**, 18 (2011) [arXiv:1001.4538 [astro-ph.CO]].
- [31] M. Battaglia *et al.*, Eur. Phys. J. C **22**, 535 (2001) [arXiv:hep-ph/0106204]; M. Battaglia, A. De Roeck, J. R. Ellis, F. Gianotti, K. A. Olive and L. Pape, Eur. Phys. J. C **33**, 273 (2004) [arXiv:hep-ph/0306219].
- [32] J. R. Ellis, T. Falk and K. A. Olive, Phys. Lett. B **444** (1998) 367 [arXiv:hep-ph/9810360]; J. R. Ellis, T. Falk, K. A. Olive and M. Srednicki, Astropart. Phys. **13** (2000) 181 [Erratum-ibid. **15** (2001) 413] [arXiv:hep-ph/9905481]; R. Arnowitt, B. Dutta and Y. Santoso, Nucl. Phys. B **606** (2001) 59 [arXiv:hep-ph/0102181]; M. E. Gómez, G. Lazarides and C. Pallis, Phys. Rev. D **D61** (2000) 123512 [arXiv:hep-ph/9907261]; Phys. Lett. **B487** (2000) 313 [arXiv:hep-ph/0004028]; Nucl. Phys. B **B638** (2002) 165 [arXiv:hep-ph/0203131]; T. Nihei, L. Roszkowski and R. Ruiz de Austri, JHEP **0207** (2002) 024 [arXiv:hep-ph/0206266].
- [33] J. L. Feng, K. T. Matchev and T. Moroi, Phys. Rev. Lett. **84**, 2322 (2000) [arXiv:hep-ph/9908309], and Phys. Rev. D **61**, 075005 (2000) [arXiv:hep-ph/9909334]; J. L. Feng, K. T. Matchev and F. Wilczek, Phys. Lett. B **482**, 388 (2000) [arXiv:hep-ph/0004043].
- [34] Joint LEP 2 Supersymmetry Working Group, *Combined LEP Chargino Results, up to 208 GeV*, http://lepsusy.web.cern.ch/lepsusy/www/inos_moriond01/charginos_pub.html.; R. Barate *et al.* [ALEPH, DELPHI, L3, OPAL Collaborations: the LEP

- Working Group for Higgs boson searches], Phys. Lett. B **565**, 61 (2003) [arXiv:hep-ex/0306033]; D. Zer-Zion, *Prepared for 32nd International Conference on High-Energy Physics (ICHEP 04), Beijing, China, 16-22 Aug 2004*; LHWG-NOTE-2004-01, ALEPH-2004-008, DELPHI-2004-042, L3-NOTE-2820, OPAL-TN-744, http://lephiggs.web.cern.ch/LEPHIGGS/papers/August2004_MSSM/index.html.
- [35] CMS Collaboration, <https://twiki.cern.ch/twiki/bin/view/CMSPublic/PhysicsResultsSUS> and references given there; ATLAS Collaboration, <https://twiki.cern.ch/twiki/bin/view/AtlasPublic/SupersymmetryPublicResults> and references given there.
- [36] J. F. Navarro, C. S. Frenk and S. D. M. White, *Astrophys. J.* **462** (1996) 563 [arXiv:astro-ph/9508025]; J. F. Navarro, C. S. Frenk and S. D. M. White, *Astrophys. J.* **490** (1997) 493 [arXiv:astro-ph/9611107].
- [37] J. Einasto, “Influence of the atmospheric and instrumental dispersion on the brightness distribution in a galaxy, *Trudy Inst. Astrofiz. Alma-Ata* **51** (1965) 87.
- [38] A. W. Graham, D. Merritt, B. Moore, J. Diemand and B. Terzic, *Astron. J.* **132** (2006) 2685 [arXiv:astro-ph/0509417]; *Astron. J.* **132** (2006) 2701 [arXiv:astro-ph/0608613]; *Astron. J.* **132** (2006) 2711 [arXiv:astro-ph/0608614].
- [39] J. N. Bahcall and R. M. Soneira, *Astrophys. J. Suppl.* **44** (1980) 73; K. G. Begeman, A. H. Broeils and R. H. Sanders, *Mon. Not. Roy. Astron. Soc.* **249** (1991) 523.
- [40] M. Srednicki, R. Watkins and K. A. Olive, *Nucl. Phys. B* **310**, 693 (1988).
- [41] J. Hisano, S. Matsumoto and M. M. Nojiri, *Phys. Rev. Lett.* **92** (2004) 031303 [arXiv:hep-ph/0307216]; J. Hisano, S. Matsumoto, M. M. Nojiri and O. Saito, *Phys. Rev. D* **71** (2005) 063528 [arXiv:hep-ph/0412403].
- [42] A. Hryczuk, *Phys. Lett. B* **699** (2011) 271 [arXiv:1102.4295 [hep-ph]].
- [43] O. Buchmueller *et al.*, *JHEP* **0809** (2008) 117 [arXiv:0808.4128 [hep-ph]]; O. Buchmueller *et al.*, *Eur. Phys. J. C* **64**, 391 (2009) [arXiv:0907.5568 [hep-ph]]; O. Buchmueller *et al.*, *Eur. Phys. J. C* **71**, 1634 (2011) [arXiv:1102.4585 [hep-ph]].
- [44] T. Sjostrand, S. Mrenna, P. Z. Skands, *JHEP* **0605** (2006) 026 [hep-ph/0603175].

- [45] S. Moretti, K. Odagiri, P. Richardson, M. H. Seymour, B. R. Webber, *JHEP* **0204** (2002) 028 [[hep-ph/0204123](#)].
- [46] J. A. R. Cembranos, A. de la Cruz-Dombriz, A. Dobado, R. A. Lineros, A. L. Maroto, *Phys. Rev.* **D83** (2011) 083507 [[arXiv:1009.4936 \[hep-ph\]](#)].
- [47] M. Cirelli, G. Corcella, A. Hektor, G. Hutsi, M. Kadastik, P. Panci, M. Raidal, F. Sala *et al.*, *JCAP* **1103** (2011) 051. [[arXiv:1012.4515 \[hep-ph\]](#)].
- [48] R. Flores, K. A. Olive and S. Rudaz, *Phys. Lett. B* **232**, 377 (1989); N. F. Bell, J. B. Dent, T. D. Jacques and T. J. Weiler, *Phys. Rev. D* **78**, 083540 (2008) [[arXiv:0805.3423 \[hep-ph\]](#)]; P. Ciafaloni, D. Comelli, A. Riotto, F. Sala, A. Strumia, A. Urbano, *JCAP* **1103** (2011) 019 [[arXiv:1009.0224 \[hep-ph\]](#)]; N. F. Bell, J. B. Dent, T. D. Jacques and T. J. Weiler, *Phys. Rev. D* **83**, 013001 (2011) [[arXiv:1009.2584 \[hep-ph\]](#)]; N. F. Bell, J. B. Dent, T. D. Jacques and T. J. Weiler, [arXiv:1101.3357 \[hep-ph\]](#). P. Ciafaloni, M. Cirelli, D. Comelli, A. De Simone, A. Riotto, A. Urbano, [[arXiv:1104.2996 \[hep-ph\]](#)]; N. F. Bell, J. B. Dent, A. J. Galea, T. D. Jacques, L. M. Krauss and T. J. Weiler, [arXiv:1104.3823 \[hep-ph\]](#).
- [49] M. Su, T. R. Slatyer and D. P. Finkbeiner, *Astrophys. J.* **724** (2010) 1044 [[arXiv:1005.5480 \[astro-ph.HE\]](#)].
- [50] R. M. Crocker, D. I. Jones, F. Aharonian, C. J. Law, F. Melia, T. Oka and J. Ott, *Mon. Not. Roy. Astron. Soc.* **413** (2011) 763 [[arXiv:1011.0206 \[astro-ph.GA\]](#)]; M. Regis, [arXiv:1101.5524 \[astro-ph.HE\]](#).
- [51] G. Bertone, M. Cirelli, A. Strumia, M. Taoso, *JCAP* **0903** (2009) 009. [[arXiv:0811.3744 \[astro-ph\]](#)].
- [52] L. Bergstrom, P. Ullio, *Nucl. Phys.* **B504** (1997) 27-44. [[hep-ph/9706232](#)].
- [53] P. Ullio and L. Bergstrom, *Phys. Rev. D* **57** (1998) 1962 [[hep-ph/9707333](#)].
- [54] H. Yuksel, S. Horiuchi, J. F. Beacom, S. 'i. Ando, *Phys. Rev.* **D76** (2007) 123506 [[arXiv:0707.0196 \[astro-ph\]](#)].
- [55] B. Moore, T. R. Quinn, F. Governato, J. Stadel and G. Lake, *Mon. Not. Roy. Astron. Soc.* **310** (1999) 1147 [[arXiv:astro-ph/9903164](#)].

- [56] A. Burkert, IAU Symp. **171** (1996) 175 [Astrophys. J. **447** (1995) L25] [arXiv:astro-ph/9504041]; A. V. Kravtsov, A. A. Klypin, J. S. Bullock and J. R. Primack, Astrophys. J. **502** (1998) 48 [arXiv:astro-ph/9708176].
- [57] R. A. Flores and J. R. Primack, Astrophys. J. **427** (1994) L1 [arXiv:astro-ph/9402004]; G. Gentile, P. Salucci, U. Klein, D. Vergani and P. Kalberla, Mon. Not. Roy. Astron. Soc. **351** (2004) 903 [arXiv:astro-ph/0403154].
- [58] J. Diemand, M. Kuhlen, P. Madau, M. Zemp, B. Moore, D. Potter and J. Stadel, Nature **454** (2008) 735 [arXiv:0805.1244 [astro-ph]].
- [59] V. Springel *et al.*, Mon. Not. Roy. Astron. Soc. **391** (2008) 1685 [arXiv:0809.0898 [astro-ph]].
- [60] J. F. Navarro *et al.*, arXiv:0810.1522 [astro-ph].
- [61] A. W. Strong, I. V. Moskalenko and O. Reimer, Astrophys. J. **537** (2000) 763 [Erratum-ibid. **541** (2000) 1109] [arXiv:astro-ph/9811296].
- [62] R. M. Crocker, D. Jones, F. Melia, J. Ott and R. J. Protheroe, Nature **468**, 65 (2010) [arXiv:1001.1275 [astro-ph.GA]].
- [63] K. Ferriere, W. Gillard and P. Jean, Astron. Astrophys. **467** (2007) 611 [arXiv:astro-ph/0702532].
- [64] T. Delahaye, R. Lineros, F. Donato, N. Fornengo, P. Salati, Phys. Rev. **D77** (2008) 063527. [arXiv:0712.2312 [astro-ph]].
- [65] A. E. Vladimirov, S. W. Digel, G. [] I. Johannesson, P. F. Michelson, I. V. Moskalenko, P. L. Nolan, E. Orlando, T. A. Porter *et al.*, Comput. Phys. Commun. **182** (2011) 1156-1161. [arXiv:1008.3642 [astro-ph.HE]].
- [66] D. Maurin, F. Donato, R. Taillet and P. Salati, Astrophys. J. **555** (2001) 585 [arXiv:astro-ph/0101231].
- [67] J. Ellis, K. A. Olive, C. Savage and V. C. Spanos, Phys. Rev. D **81**, 085004 (2010) [arXiv:0912.3137 [hep-ph]].
- [68] A. W. Strong and I. V. Moskalenko, Astrophys. J. **509** (1998) 212 [arXiv:astro-ph/9807150]; I. V. Moskalenko and A. W. Strong, Astrophys. J. **493** (1998) 694 [arXiv:astro-ph/9710124].

- [69] S. D. Hunter *et al.*, *Astrophys. J.* **481**, 205 (1997).
- [70] A. W. Strong, I. V. Moskalenko and O. Reimer, *Astrophys. J.* **613** (2004) 956 [arXiv:astro-ph/0405441]; A. W. Strong, I. V. Moskalenko and O. Reimer, *Astrophys. J.* **613** (2004) 962 [arXiv:astro-ph/0406254].
- [71] F. W. Stecker and M. H. Salamon, *Astrophys. J.* **464** (1996) 600 [arXiv:astro-ph/9601120]; V. Pavlidou and B. D. Fields, *Astrophys. J.* **575** (2002) L5 [arXiv:astro-ph/0207253]; S. Gabici and P. Blasi, *Astropart. Phys.* **19** (2003) 679 [arXiv:astro-ph/0211573]; T. Totani, *Astropart. Phys.* **11** (1999) 451 [arXiv:astro-ph/9810207]; A. Loeb and E. Waxman, *Nature* **405** (2000) 156 [arXiv:astro-ph/0003447]; O. E. Kalashev, D. V. Semikoz and G. Sigl, *Phys. Rev. D* **79** (2009) 063005 [arXiv:0704.2463 [astro-ph]].
- [72] P. Sreekumar *et al.* [EGRET Collaboration], *Astrophys. J.* **494** (1998) 523 [arXiv:astro-ph/9709257].
- [73] <http://fermi.gsfc.nasa.gov/ssc/data/analysis/scitools/>.